Secrecy Energy Efficiency in Cognitive Radio Networks With Untrusted Secondary Users

Wei-Bang Wang, Yang Lu, *Member, IEEE*, and Chong-Yung Chi, *Life Fellow, IEEE*

***Abstract*—The information security and energy efficiency in cognitive radio (CR) networks have been extensively studied. However, the practical scenario involving multiple untrusted secondary users (SUs) in CR networks under the underlay spectrum sharing mechanism has not been studied so far. This article considers the downlink secrecy energy efficient coordinated beamforming design for multiple inputs single output CR networks under this scenario. Our goal is to maximize the global secrecy energy efficiency (GSEE), defined as the ratio of the sum of secrecy rates of all the primary users (PUs) to the total power consumption, under requirements on quality of service of PUs and SUs as well as constraints on power budget at the primary transmitter (PTx) and the secondary transmitter (STx). To tackle the non-convex GSEE maximization (GSEEM) problem, an algorithm is proposed based on Dinkelbach method and successive convex approximation to jointly optimize beamforming vectors of the PTx and the STx. The convergence behavior and the computational complexity of the proposed GSEEM algorithm are analyzed, followed by the connection with the secrecy rate maximization design and the power minimization (PM) design in terms of GSEE. In view of significantly higher computational complexity of the proposed GSEEM algorithm than that of the PM design, a 2-step searching scheme is further designed to efficiently search for an approximate solution to the considered GSEEM problem based on the PM design and the golden search method. Simulation results demonstrate the efficacy of the proposed GSEEM algorithm and the searching scheme, and show that the spatial degrees of freedom (primarily determined by the antenna numbers of PTx and STx) is the key factor to the performance of the proposed GSEEM algorithm.**

***Index Terms*—Secrecy energy efficiency, cognitive radio, fractional programming, successive convex approximation.**

I. Introduction

THE RAPID development of the information and communication technology (ICT) causes significant growth of the energy consumption in ICT industry. It has been reported that ICT industry will account for 3.6% of the global greenhouse gas emission by 2020 and for 14% by 2040 [1]. To mitigate the adverse impact on the environment and reduce the operating expenditures due to energy consumption, green communication has become a central consideration in both academia and industry, which makes energy efficiency (EE) an essential performance metric in designing wireless communication networks [2], [3]. Developing energy-efficient ICT can also prolong the operation lifetime of battery-limited devices such as sensors in Internet of Things. Therefore, the EE maximization design for transmitting as many bits as possible per unit of energy has been regarded as a fundamental consideration in many application scenarios [4], [5].

On the other hand, the explosive growth of data traffic is straining the limited spectrum resource. It is estimated that the mobile data traffic demand will increase by more than 160% from 2019 to 2022 [6]. In view of the conflicts between the limited spectrum resource and the increasing data traffic demand, cognitive radio (CR) has been proposed for improving spectrum efficiency [7], [8]. By dynamic spectrum sharing, secondary users (SUs), i.e., unlicensed users, are allowed to access the wireless networks via the underutilized spectrum as long as the information transmission of SUs by the secondary transmitter (STx) would not cause adverse effects on the quality of service (QoS) of primary users (PUs), i.e., licensed users, served by the primary transmitter (PTx) [9], [10]. The performance of CR networks highly depends on the spectrum sharing schemes [11]. Two single-hop spectrum sharing schemes have been widely investigated in the literature, i.e., the interweave spectrum sharing (ISS) and the underlay spectrum sharing (USS) [12], [13]. For the former, the STx-SU links are allowed to operate over their detected spectrum holes. For the latter, the STx-SU links are allowed to operate concurrently with the PTx-PU links if their interference to the PTx-PU links is suppressed below an interference temperature limit. Compared with the USS, the ISS may not work as expected especially for multi-user scenarios due to the following reasons. First, under the practical scenario of massive devices accessing the networks, it becomes difficult to detect spectrum holes for SUs. Second, once the spectrum detection or geolocation database involves errors on the state of the spectrum occupancy, severe cochannel interference may bring about among PUs and SUs. Third, when the PTx-PU links re-utilize the spectrum, the operation of the STx-SU links must be shut down immediately, thus making their transmission unreliable. Alternatively, with the USS, the information signals of SUs can be thought of as jamming signals to

Manuscript received February 21, 2020; revised July 29, 2020 and September 19, 2020; accepted October 6, 2020. Date of publication October 14, 2020; date of current version March 18, 2021. This work was supported in part by the Ministry of Science and Technology, ROC, under Grant MOST 107-2221-E-007-021, Grant MOST 108-2221-E-007-012, and Grant MOST 109-2221-E007-088, and in part by the General Program of the National Natural Science Foundation of China under Grant 62071033. The associate editor coordinating the review of this article and approving it for publication was K. Adachi. *(Corresponding authors: Wei-Bang Wang; Yang Lu.)*

Wei-Bang Wang and Chong-Yung Chi are with the Institute of Communications Engineering, Department of Electrical Engineering, National Tsing Hua University, Hsinchu 30013, Taiwan (e-mail: s107064529@m107.nthu.edu.tw; cychi@ee.nthu.edu.tw).

Yang Lu is with the School of Computer and Information Technology, Beijing Jiaotong University, Beijing 100044, China (e-mail: yanglu@bjtu.edu.cn).

Digital Object Identifier 10.1109/TGCN.2020.3031036

confuse the malicious eavesdroppers who intend to intercept the information for PUs [14].

Nevertheless, the QoS of PUs may be degraded due to the interference introduced by the STx-PU links. Besides, allowing SUs to access the networks may increase the risk of information leakage from PUs to SUs because of the broadcast nature of wireless communications [15]–[17]. Therefore, the interference management and information security are two critical issues in the USS-based CR networks. To handle these challenging issues, the multi-antenna technology is regarded as one of the most promising technologies [18]–[20]. By aiming the information beamformer at the direction of the specific users, the interference of STx-PU links can be effectively mitigated and meanwhile the information leakage from PUs to SUs can be reduced. Moreover, the multi-antenna technology is also popular in energy-efficient designs by making use of sufficient spatial degrees of freedom (DoF). Thus, jointly enhancing the information security and EE has become a central goal in multi-antenna CR networks.

So far, the information security and EE for multi-antenna CR networks have been widely investigated in the literature [21]–[30]. In [21] for perfect channel state information (CSI), and [22] for imperfect CSI, the transmit beamforming designs were studied for multiple inputs single output (MISO) CR networks to maximize the secrecy rate under constraints of the transmit power budget and the tolerable interference to PUs, but EE was not taken into account. In [23], EE was maximized for multi-user secure CR networks while satisfying the secrecy information rate requirement of each PU. To balance the information security and EE, secrecy EE (SEE), defined as the ratio of the secrecy rate to the total power consumption, is considered as a useful performance metric. In [24]–[28], SEE was maximized for secure CR networks in the presence of malicious eavesdroppers under different scenarios with various system requirements. However, in practical CR networks, due to the openness of spectrum, even without malicious eavesdroppers, PUs' information security is still vulnerable to SUs [29]. Besides, if malicious eavesdroppers disguise as legitimate SUs, it would be easy for them to intercept PUs' information. In [30], the optimal power allocation scheme was studied for a CR network for the single-user case (one PU and one SU) with the SU treated as a potential eavesdropper. However, the designed scheme for such single-user case cannot be applied to the multi-user case. As for the general scenario of multiple PUs and multiple untrusted SUs in CR networks, the beamforming design for maximum SEE is still a challenging open problem, that motivates the proposed study in our work.

In this article, we investigate the coordinated beamforming design for multi-PU MISO USS-based CR networks in the presence of multiple untrusted SUs. To further guarantee the information security, assume that the receivers of SUs (potential eavesdroppers) are equipped with the successive interference cancellation function for decoding the received signals from the PTx. The main contributions of this article are summarized as follows.

- In order to explore the global SEE (GSEE) performance limit of CR networks, a downlink coordinated transmit beamforming design problem is formulated to maximize GSEE subject to the QoS requirements of PUs and SUs as well as the power budget of PTx and STx. *To the best of our knowledge, the GSEE performance for multi-user multi-antenna USS-based CR networks has not been reported in the open literature.*
- To efficiently solve the considered non-convex problem, a dual-layer iterative GSEE maximization (GSEEM) algorithm (named Algorithm 2) is proposed based on Dinkelbach method [31] in the inner loop and successive convex approximation (SCA) [32], [33] in the outer loop. Apart from the complexity analysis of Algorithm 2, it is theoretically proved that the designed transmit beamformers of PTx and STx obtained by Algorithm 2 converge to a Karush-Kuhn-Tucker (KKT) point of the semidefinite relaxation (SDR) of the considered problem. Note that the proposed Algorithm 2 is also a general GSEEM framework which is applicable not only to CR networks but also to other multi-user multi-antenna networks.
- The connection between the proposed GSEEM design and two traditional designs, i.e., the secrecy rate maximization (SRM) design [34] and the power minimization (PM) design [35], is analyzed, thereby leading to the finding that the computationally efficient PM design and Algorithm 2 have quite comparable GSEE performance when the target QoS requirement for PUs exceeds a certain threshold. Thanks to this finding, we further propose a PM based searching scheme (PMBSS) (named Algorithm 3) using the PM design and the golden search method [36] to efficiently find a surrogate solution to the considered GSEEM problem.
- Abundant simulation results are provided to demonstrate the efficacy of the proposed Algorithm 2 and Algorithm 3 and validate the proposed analysis results. Simulation results also show that sufficient spatial DoF (primarily determined by the antenna numbers of PTx and STx) is the key factor to the performance of Algorithm 2.

The rest of this article is organized as follows. Section II presents the signal model and problem statement. The proposed GSEEM algorithm is presented in Section III followed by computational complexity and performance analysis. The PMBSS algorithm is presented in Section IV. Simulation results are provided in Section V. Finally, Section VI concludes the paper.

Notation: Matrices and vectors are denoted by uppercase and lowercase boldface letters, $\mathbf{X}$ and $\mathbf{x}$, respectively. $\mathbb{C}^n$ and $\mathbb{H}^n$ are the sets of $n \times 1$ complex vectors and complex $n \times n$ Hermitian matrices, respectively. $\mathbf{X}^H$ ($\mathbf{x}^H$) denotes the conjugate transpose of matrix $\mathbf{X}$ (vector $\mathbf{x}$). $\mathbf{A} \succeq \mathbf{0}$ means that $\mathbf{A}$ is a positive semidefinite (PSD) matrix. Tr($\mathbf{A}$) is the trace of square matrix $\mathbf{A}$. $\lambda_{\max}(\mathbf{A})$ denotes the maximum eigenvalue of PSD matrix $\mathbf{A}$. $\mathbf{I}_n$ denotes the $n \times n$ identity matrix. $[\mathbf{A}]_{ij}$ stands for the (*i*,*j*)th entry of $\mathbf{A}$. $\mathbb{E}\{\cdot\}$ denotes the expectation operator; $\|\cdot\|$ denotes the Euclidean norm; and $[x]^+$ denotes the maximum of 0 and $x \in \mathbb{R}$. $\{\mathbf{x}_i\}$ stands for the set of $\mathbf{x}_i$ with all the admissible *i*, so does $\{\mathbf{x}_{i,j}\}$ with all the admissible *i*, *j*; $\{\mathbf{x}_i\}_{i\neq k}$ stands for the set $\{\mathbf{x}_i\}$ excluding $\mathbf{x}_k$.

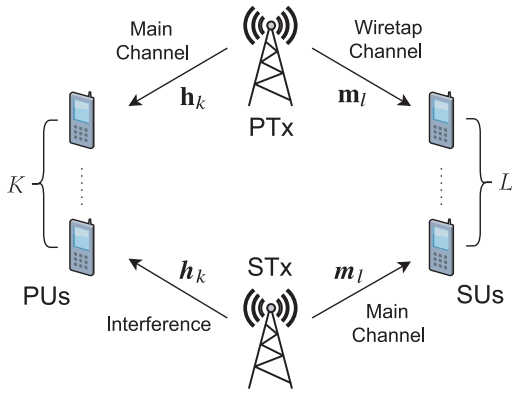

Fig. 1. The considered scenario of the USS-based CR networks with multiple PUs and multiple untrusted SUs.

II. Signal Model and Problem Statement

Consider a multi-user downlink CR networks operating under the USS mechanism as shown in Fig. 1, where an $N_{\rm P}$-antenna PTx serves K single-antenna PUs and an $N_{\rm S}$-antenna STx serves L single-antenna SUs, but all the SUs are implicitly treated as eavesdroppers without collusion among them. Moreover, all the CSI (i.e., $\{\mathbf{h}_k, \boldsymbol{h}_k\}, \{\mathbf{m}_l, \boldsymbol{m}_l\}$) are assumed perfectly known. To guarantee the QoS of PUs and SUs, the coordinated beamforming design is employed.

Let ϑ_k and ζ_l denote the information-bearing signals for the k-th PU and l-th SU, respectively, and they are assumed to be Gaussian, where $k \in \mathbb{K} \coloneqq \{1, \ldots, K\}$ and $l \in \mathbb{L} \coloneqq \{1, \ldots, L\}$. Without loss of generality, let $\mathbb{E}\{|\vartheta_k|^2\} = 1$ and $\mathbb{E}\{|\zeta_l|^2\} = 1$. In each time slot, the transmit signals of PTx and STx can be respectively expressed as the following Gaussian random vectors

$$\mathbf{x} = \sum_{k=1}^{K} \mathbf{v}_k \vartheta_k \ \text{ and } \ \boldsymbol{x} = \sum_{l=1}^{L} \boldsymbol{w}_l \zeta_l,$$

where $\mathbf{v}_k \in \mathbb{C}^{N_{\rm P}}$ and $\boldsymbol{w}_l \in \mathbb{C}^{N_{\rm S}}$ denote the beamforming vectors associated with the k-th PU and the l-th SU, respectively. Then, the total power consumption at PTx and STx can be expressed as

$$P_{\rm T}\big(\{\mathbf{v}_i\}, \{\boldsymbol{w}_j\}\big) = P_{\rm actual}\big(\{\mathbf{v}_i\}, \{\boldsymbol{w}_j\}\big) + P_{\rm c} \tag{1}$$

where $P_{\rm c}$ is the circuit power consumed by PTx and STx, and

$$P_{\rm actual}\big(\{\mathbf{v}_i\}, \{\boldsymbol{w}_j\}\big) = \sum_{k=1}^{K} \|\mathbf{v}_k\|^2 + \sum_{l=1}^{L} \|\boldsymbol{w}_l\|^2 \tag{2}$$

is the power used for information transmission.

For the k-th PU, the received signal is given by

$$\begin{aligned} y_k^{(\rm p)} &= \mathbf{h}_k^H \mathbf{x} + \boldsymbol{h}_k^H \boldsymbol{x} + n_k \\ &= \underbrace{\mathbf{h}_k^H \mathbf{v}_k \vartheta_k}_{\text{Desired signal}} + \underbrace{\sum_{i \in \mathbb{K}\setminus\{k\}} \mathbf{h}_k^H \mathbf{v}_i \vartheta_i + \sum_{l=1}^{L} \boldsymbol{h}_k^H \boldsymbol{w}_l \zeta_l}_{\text{Interference}} + n_k, \end{aligned} \tag{3}$$

where $\mathbf{h}_k \in \mathbb{C}^{N_{\rm P}}$ and $\boldsymbol{h}_k \in \mathbb{C}^{N_{\rm S}}$ denote the channel vectors, one between the PTx and the k-th PU, and the other between the STx and the k-th PU; $n_k \sim \mathcal{CN}(0, \sigma_k^2)$ denotes the additive white Gaussian noise (AWGN). By (3), the achievable rate at the k-th PU is given by

$$\begin{aligned} &R_k^{(\rm p)}(\{\mathbf{v}_i\}, \{\boldsymbol{w}_j\}) \\ &= \log_2\left(1 + \frac{\left|\mathbf{h}_k^H \mathbf{v}_k\right|^2}{\sum_{i \in \mathbb{K}\setminus\{k\}} \left|\mathbf{h}_k^H \mathbf{v}_i\right|^2 + \sum_{l=1}^{L} \left|\boldsymbol{h}_k^H \boldsymbol{w}_l\right|^2 + \sigma_k^2}\right). \end{aligned} \tag{4}$$

Similarly, the received signal at the l-th SU is

$$y_l^{(\rm s)} = \boldsymbol{m}_l^H \boldsymbol{w}_l \zeta_l + \sum_{j \in \mathbb{L}\setminus\{l\}} \boldsymbol{m}_l^H \boldsymbol{w}_j \zeta_j + \sum_{k=1}^{K} \mathbf{m}_l^H \mathbf{v}_k \vartheta_k + n_l, \tag{5}$$

where $\boldsymbol{m}_l \in \mathbb{C}^{N_{\rm S}}$ and $\mathbf{m}_l \in \mathbb{C}^{N_{\rm P}}$ denote the channel vectors, one between the STx and the l-th SU, and the other between the PTx and the l-th SU; and $n_l \sim \mathcal{CN}(0, \rho_l^2)$ is AWGN. By (5), the achievable rate at the l-th SU is given by

$$\begin{aligned} &R_l^{(\rm s)}(\{\mathbf{v}_i\}, \{\boldsymbol{w}_j\}) \\ &= \log_2\left(1 + \frac{\left|\boldsymbol{m}_l^H \boldsymbol{w}_l\right|^2}{\sum_{k=1}^{K} \left|\mathbf{m}_l^H \mathbf{v}_k\right|^2 + \sum_{j \in \mathbb{L}\setminus\{l\}} \left|\boldsymbol{m}_l^H \boldsymbol{w}_j\right|^2 + \rho_l^2}\right). \end{aligned} \tag{6}$$

Suppose that the l-th SU attempts to eavesdrop the information intended for the k-th PU, an upper bound[1] of the associated achievable rate at the l-th SU is given by

$$\begin{aligned} &R_{k,l}^{(\rm Eve)}\Big(\{\mathbf{v}_i\}, \{\boldsymbol{w}_j\}_{j \neq l}\Big) \\ &= \log_2\left(1 + \frac{\left|\mathbf{m}_l^H \mathbf{v}_k\right|^2}{\sum_{i \in \mathbb{K}\setminus\{k\}} \left|\mathbf{m}_l^H \mathbf{v}_i\right|^2 + \sum_{j \in \mathbb{L}\setminus\{l\}} \left|\boldsymbol{m}_l^H \boldsymbol{w}_j\right|^2 + \rho_l^2}\right). \end{aligned} \tag{7}$$

Then, the corresponding secrecy rate for the k-th PU [24], [37] is given by

$$\begin{aligned} &R_{k,l}^{(\rm Sec)}\big(\{\mathbf{v}_i\}, \{\boldsymbol{w}_j\}\big) \\ &= \Big[R_k^{(\rm p)}\big(\{\mathbf{v}_i\}, \{\boldsymbol{w}_j\}\big) - R_{k,l}^{(\rm Eve)}\Big(\{\mathbf{v}_i\}, \{\boldsymbol{w}_j\}_{j \neq l}\Big)\Big]^+. \end{aligned} \tag{8}$$

For the considered system, the GSEE [38], [39] (measured in bit/Hz/J) is defined as

$$\mathrm{GSEE}\big(\{\mathbf{v}_i\}, \{\boldsymbol{w}_j\}\big) = \frac{\mathcal{R}^{(\rm Sec)}\big(\{\mathbf{v}_i\}, \{\boldsymbol{w}_j\}\big)}{P_{\rm T}\big(\{\mathbf{v}_i\}, \{\boldsymbol{w}_j\}\big)} \tag{9}$$

where

$$\mathcal{R}^{(\rm Sec)}\big(\{\mathbf{v}_i\}, \{\boldsymbol{w}_j\}\big) = \sum_{l=1}^{L} \sum_{k=1}^{K} R_{k,l}^{(\rm Sec)}\big(\{\mathbf{v}_i\}, \{\boldsymbol{w}_j\}\big) \tag{10}$$

is the sum of the secrecy rates of all the PUs because for any pair of $\{k, l\}$, there is just one corresponding secrecy

[1]The upper bound given by (7) can be achieved provided that the l-th SU is able to suppress the target signal $\boldsymbol{m}_l^H \boldsymbol{w}_l \zeta_l$ in (5) by applying successive interference cancellation to the received signal given by (5).

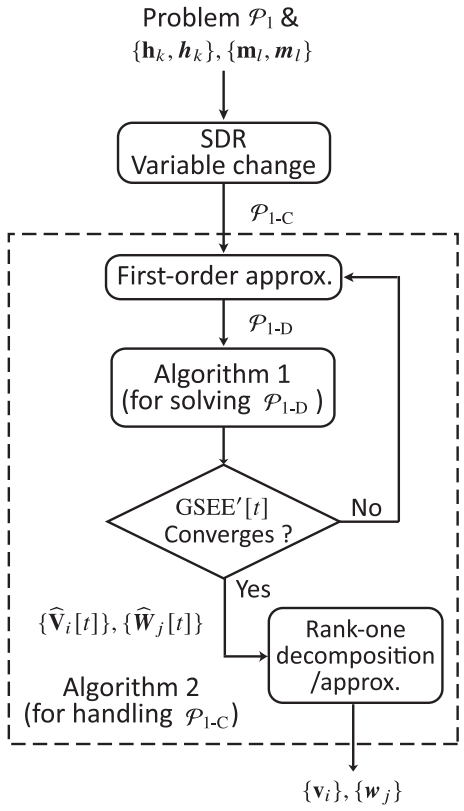

Fig. 2. Processing structure of the proposed GSEEM Algorithm (Algorithm 2), an SCA based algorithm for handling $\mathcal{P}_{1\text{-C}}$, where Algorithm 1 is designed for solving $\mathcal{P}_{1\text{-D}}$ by Dinkelbach method.

rate due to no collusion among all the SUs (eavesdroppers). An optimization problem for maximizing GSEE is formulated as

$$\begin{aligned}\mathcal{P}_1\colon \max\ & \mathrm{GSEE}\big(\{\mathbf{v}_i\},\{\boldsymbol{w}_j\}\big)\\ \text{s.t.}\ & R_k^{(\mathrm{p})}\big(\{\mathbf{v}_i\},\{\boldsymbol{w}_j\}\big)\geq \mathcal{Q}_k^{(\mathrm{p})},\ \forall k\in\mathbb{K} \quad (11a)\\ & R_l^{(\mathrm{s})}\big(\{\mathbf{v}_i\},\{\boldsymbol{w}_j\}\big)\geq \mathcal{Q}_l^{(\mathrm{s})},\ \forall l\in\mathbb{L} \quad (11b)\\ & P_{\mathrm{T}}\big(\{\mathbf{v}_i\},\{\boldsymbol{w}_j\}\big)\leq P_{\max}, \quad (11c)\end{aligned}$$

where $\mathcal{Q}_k^{(\mathrm{p})}$ and $\mathcal{Q}_l^{(\mathrm{s})}$ are the minimum rate requirements of the k-th PU and the l-th SU, respectively, and $P_{\max}$ is the power budget of PTx and STx.

The considered problem is hard to solve due to the non-convex fractional objective function, and the non-convex constraints (11a) and (11b). In the next section, we propose an algorithm for finding a good approximate solution to the GSEEM problem $\mathcal{P}_1$.

III. The Proposed GSEEM Algorithm

A. Algorithm Design

The approach for handling $\mathcal{P}_1$ is to apply SDR followed by change of variables and first-order convex approximation such that the resulting approximate problem $\mathcal{P}_{1\text{-D}}$ (see (24)) has a convex feasible set, although its objective function is still a non-convex fractional function. Then, Dinkelbach method (to be implemented by Algorithm 1) can be used to efficiently solve $\mathcal{P}_{1\text{-D}}$ together with the use of the SCA for handling $\mathcal{P}_{1\text{-C}}$ (see (21)). Thus, we come up with the proposed GSEEM Algorithm (i.e., Algorithm 2) with the processing structure as shown in Fig. 2. Next, we focus on problem formulations involved in Algorithm 2.

Letting $\mathbf{V}_k = \mathbf{v}_k\mathbf{v}_k^H \in \mathbb{H}^{N_{\mathrm{p}}}$ and $\boldsymbol{W}_l = \boldsymbol{w}_l\boldsymbol{w}_l^H \in \mathbb{H}^{N_{\mathrm{s}}}$ (rank-one PSD matrices), the total power consumption P_{T} given by (1) and the achievable rates $R_k^{(\mathrm{p})}$, $R_l^{(\mathrm{s})}$, and $R_{k,l}^{(\mathrm{Eve})}$ given by (4), (6), and (7) can be respectively rewritten as

$$\begin{aligned}&P_{\mathrm{T}}(\{\mathbf{V}_i\},\{\boldsymbol{W}_j\}) = \mathrm{Tr}\Big(\sum_{k=1}^{K}\mathbf{V}_k\Big)+\mathrm{Tr}\Big(\sum_{l=1}^{L}\boldsymbol{W}_l\Big)+P_{\mathrm{c}},\\ &R_k^{(\mathrm{p})}(\{\mathbf{V}_i\},\{\boldsymbol{W}_j\})\\ &\quad=\log_2\left(1+\frac{\mathbf{h}_k^H\mathbf{V}_k\mathbf{h}_k}{\sum_{i\in\mathbb{K}\setminus\{k\}}\mathbf{h}_k^H\mathbf{V}_i\mathbf{h}_k+\sum_{l=1}^{L}\boldsymbol{h}_k^H\boldsymbol{W}_l\boldsymbol{h}_k+\sigma_k^2}\right),\\ &R_l^{(\mathrm{s})}(\{\mathbf{V}_i\},\{\boldsymbol{W}_j\})\\ &\quad=\log_2\left(1+\frac{\boldsymbol{m}_l^H\boldsymbol{W}_l\boldsymbol{m}_l}{\sum_{k=1}^{K}\mathbf{m}_l^H\mathbf{V}_k\mathbf{m}_l+\sum_{j\in\mathbb{L}\setminus\{l\}}\boldsymbol{m}_l^H\boldsymbol{W}_j\boldsymbol{m}_l+\rho_l^2}\right),\\ &R_{k,l}^{(\mathrm{Eve})}\Big(\{\mathbf{V}_i\},\{\boldsymbol{W}_j\}_{j\neq l}\Big)\\ &\quad=\log_2\left(1+\frac{\mathbf{m}_l^H\mathbf{V}_k\mathbf{m}_l}{\sum_{i\in\mathbb{K}\setminus\{k\}}\mathbf{m}_l^H\mathbf{V}_i\mathbf{m}_l+\sum_{j\in\mathbb{L}\setminus\{l\}}\boldsymbol{m}_l^H\boldsymbol{W}_j\boldsymbol{m}_l+\rho_l^2}\right).\end{aligned}$$

Accordingly, the corresponding $R_{k,l}^{(\mathrm{Sec})}$ (see (8)), $\mathcal{R}^{(\mathrm{Sec})}$ (see (10)) and GSEE (see (9)) can also be respectively rewritten as

$$\begin{aligned}R_{k,l}^{(\mathrm{Sec})}\big(\{\mathbf{V}_i\},\{\boldsymbol{W}_j\}\big) &= \Big[R_k^{(\mathrm{p})}\big(\{\mathbf{V}_i\},\{\boldsymbol{W}_j\}\big)-\\ &\qquad R_{k,l}^{(\mathrm{Eve})}\Big(\{\mathbf{V}_i\},\{\boldsymbol{W}_j\}_{j\neq l}\Big)\Big]^{+}, \quad (12)\\ \mathcal{R}^{(\mathrm{Sec})}\big(\{\mathbf{V}_i\},\{\boldsymbol{W}_j\}\big) &= \sum_{l=1}^{L}\sum_{k=1}^{K}R_{k,l}^{(\mathrm{Sec})}\big(\{\mathbf{V}_i\},\{\boldsymbol{W}_j\}\big), \quad (13)\\ \mathrm{GSEE}\big(\{\mathbf{V}_i\},\{\boldsymbol{W}_j\}\big) &= \frac{\mathcal{R}^{(\mathrm{Sec})}\big(\{\mathbf{V}_i\},\{\boldsymbol{W}_j\}\big)}{P_{\mathrm{T}}\big(\{\mathbf{V}_i\},\{\boldsymbol{W}_j\}\big)}. \quad (14)\end{aligned}$$

Then, the SDR of $\mathcal{P}_1$ is given by

$$\begin{aligned}\mathcal{P}_{1\text{-A}}\colon \max\ & \mathrm{GSEE}\big(\{\mathbf{V}_i\},\{\boldsymbol{W}_j\}\big)\\ \text{s.t.}\ & R_k^{(\mathrm{p})}\big(\{\mathbf{V}_i\},\{\boldsymbol{W}_j\}\big)\geq \mathcal{Q}_k^{(\mathrm{p})}, \quad (15a)\\ & R_l^{(\mathrm{s})}\big(\{\mathbf{V}_i\},\{\boldsymbol{W}_j\}\big)\geq \mathcal{Q}_l^{(\mathrm{s})}, \quad (15b)\\ & P_{\mathrm{T}}\big(\{\mathbf{V}_i\},\{\boldsymbol{W}_j\}\big)\leq P_{\max}, \quad (15c)\\ & \mathbf{V}_k\succeq\mathbf{0},\ \boldsymbol{W}_l\succeq\mathbf{0},\ \forall k\in\mathbb{K},\ \forall l\in\mathbb{L}. \quad (15d)\end{aligned}$$

Note that (15a) and (15b) are non-convex constraints in $\mathcal{P}_{1\text{-A}}$ but they can be readily reformulated as the following two convex constraints:

$$\begin{aligned}\mathbf{h}_k^H\mathbf{V}_k\mathbf{h}_k \geq{}& \left(2^{\mathcal{Q}_k^{(\mathrm{p})}}-1\right)\\ &\times\left(\sum_{i\in\mathbb{K}\setminus\{k\}}\mathbf{h}_k^H\mathbf{V}_i\mathbf{h}_k+\sum_{l=1}^{L}\boldsymbol{h}_k^H\boldsymbol{W}_l\boldsymbol{h}_k+\sigma_k^2\right) \quad (16a)\end{aligned}$$

$$\mathbf{m}_l^H \mathbf{W}_l \mathbf{m}_l \le \left(2^{\mathcal{Q}_l^{(\mathrm{s})}} - 1\right) \times \left(\sum_{k=1}^{K} \mathbf{m}_l^H \mathbf{V}_k \mathbf{m}_l + \sum_{j \in \mathbb{L}\setminus\{l\}} \boldsymbol{m}_l^H \boldsymbol{W}_j \boldsymbol{m}_l + \rho_l^2\right) \tag{16b}$$

such that the feasible set of $\mathcal{P}_{\text{1-A}}$ is convex and composed of (16a), (16b), (15c) and (15d) instead. Furthermore, let

$$\mathrm{GSEE}'\big(\{\alpha_k\}, \{\beta_{k,l}\}, \{\mathbf{V}_i\}, \{\boldsymbol{W}_j\}\big) = \frac{\sum_{l=1}^{L}\sum_{k=1}^{K}(\alpha_k - \beta_{k,l})}{P_{\mathrm{T}}\big(\{\mathbf{V}_i\}, \{\boldsymbol{W}_j\}\big)} \tag{17}$$

where

$$\alpha_k \coloneqq R_k^{(\mathrm{p})}\big(\{\mathbf{V}_i\}, \{\boldsymbol{W}_j\}\big)$$
$$\beta_{k,l} \coloneqq R_{k,l}^{(\mathrm{Eve})}\Big(\{\mathbf{V}_i\}, \{\boldsymbol{W}_j\}_{j\neq l}\Big).$$

Note that $\mathrm{GSEE}' \le \mathrm{GSEE}$ by (17) and (14) since $\alpha_k - \beta_{k,l} \le [\alpha_k - \beta_{k,l}, 0]^+$, and that the numerator of GSEE' is affine (and concave) in $\{\alpha_k\}$ and $\{\beta_{k,l}\}$. Instead of handling $\mathcal{P}_{\text{1-A}}$, we consider the following problem

$$\begin{aligned}\mathcal{P}_{\text{1-B}}\colon \max\ & \mathrm{GSEE}'\big(\{\alpha_k\}, \{\beta_{k,l}\}, \{\mathbf{V}_i\}, \{\boldsymbol{W}_j\}\big)\\ \text{s.t.}\ & R_k^{(\mathrm{p})}\big(\{\mathbf{V}_i\}, \{\boldsymbol{W}_j\}\big) \ge \alpha_k, && \text{(18a)}\\ & R_{k,l}^{(\mathrm{Eve})}\big(\{\mathbf{V}_i\}, \{\boldsymbol{W}_j\}\big) \le \beta_{k,l}, && \text{(18b)}\\ & \text{(16a), (16b), (15c), (15d),}\end{aligned}$$

from which we come up with the fractional program $\mathcal{P}_{\text{1-D}}$ below, that can be handled by Dinkelbach method (which requires the numerator and the denominator of the objective function GSEE' to be concave and convex, respectively).

By introducing auxiliary variables $a_k, b_k, c_{k,l}$ and $d_{k,l}$, the two non-convex constraints (18a) and (18b) can be re-expressed respectively as

$$\mathbf{h}_k^H \mathbf{V}_k \mathbf{h}_k \ge \underbrace{\left(2^{\alpha_k} - 1\right)}_{\coloneqq \exp(a_k)} \times \underbrace{\left(\sum_{i\in\mathbb{K}\setminus\{k\}} \mathbf{h}_k^H \mathbf{V}_i \mathbf{h}_k + \sum_{l=1}^{L} \boldsymbol{h}_k^H \boldsymbol{W}_l \boldsymbol{h}_k + \sigma_k^2\right)}_{\coloneqq \exp(b_k)} \tag{19}$$

$$\mathbf{m}_l^H \mathbf{V}_k \mathbf{m}_l \le \underbrace{\left(2^{\beta_{k,l}} - 1\right)}_{\coloneqq \exp(c_{k,l})} \times \underbrace{\left(\sum_{i\in\mathbb{K}\setminus\{k\}} \mathbf{m}_l^H \mathbf{V}_i \mathbf{m}_l + \sum_{j\in\mathbb{L}\setminus\{l\}} \boldsymbol{m}_l^H \boldsymbol{W}_j \boldsymbol{m}_l + \rho_l^2\right)}_{\coloneqq \exp(d_{k,l})}. \tag{20}$$

Then, $\mathcal{P}_{\text{1-B}}$ can be equivalently reformulated as

$$\begin{aligned}\mathcal{P}_{\text{1-C}}\colon \max\ & \mathrm{GSEE}'\big(\{\alpha_k\}, \{\beta_{k,l}\}, \{\mathbf{V}_i\}, \{\boldsymbol{W}_j\}\big)\\ \text{s.t.}\ & \mathbf{h}_k^H \mathbf{V}_k \mathbf{h}_k \ge e^{a_k + b_k}, && \text{(21a)}\\ & e^{a_k} \ge 2^{\alpha_k} - 1, && \text{(21b)}\\ & e^{b_k} \ge \sum_{i\in\mathbb{K}\setminus\{k\}} \mathbf{h}_k^H \mathbf{V}_i \mathbf{h}_k + \sum_{l=1}^{L} \boldsymbol{h}_k^H \boldsymbol{W}_l \boldsymbol{h}_k + \sigma_k^2, && \text{(21c)}\\ & e^{c_{k,l} + d_{k,l}} \ge \mathbf{m}_l^H \mathbf{V}_k \mathbf{m}_l, && \text{(21d)}\\ & \log_2(e^{c_{k,l}} + 1) \le \beta_{k,l}, && \text{(21e)}\\ & e^{d_{k,l}} \le \sum_{i\in\mathbb{K}\setminus\{k\}} \mathbf{m}_l^H \mathbf{V}_i \mathbf{m}_l + \sum_{j\in\mathbb{L}\setminus\{l\}} \boldsymbol{m}_l^H \boldsymbol{W}_j \boldsymbol{m}_l + \rho_l^2, && \text{(21f)}\\ & \text{(16a), (16b), (15c), (15d).}\end{aligned}$$

A noteworthy remark about the two mathematically equivalent problems $\mathcal{P}_{\text{1-B}}$ and $\mathcal{P}_{\text{1-C}}$ is as follows:

Remark 1: The optimal solution to $\mathcal{P}_{\text{1-C}}$ ($\mathcal{P}_{\text{1-B}}$) is attained when the inequality constraints of (21a) through (21f) (i.e., (18a) and (18b)) hold with equality, and they share the same optimal GSEE' as well as the beamforming solution.

Although (21b)-(21d) in $\mathcal{P}_{\text{1-C}}$ are still non-convex, their left-hand sides are convex functions, and thus can be approximated by the corresponding first-order lower bounds. Let $(\{\bar{\mathbf{V}}_i\}, \{\bar{\boldsymbol{W}}_j\}, \{\bar{\alpha}_k\}, \{\bar{\beta}_{k,l}\})$ be a feasible point to $\mathcal{P}_{\text{1-B}}$. Let $\bar{a}_k \coloneqq \ln(2^{\bar{\alpha}_k} - 1)$, $\bar{c}_k \coloneqq \ln(2^{\bar{\beta}_k} - 1)$ and

$$\bar{b}_k \coloneqq \ln\left(\sum_{i\in\mathbb{K}\setminus\{k\}} \mathbf{h}_k^H \bar{\mathbf{V}}_i \mathbf{h}_k + \sum_{l=1}^{L} \boldsymbol{h}_k^H \bar{\boldsymbol{W}}_l \boldsymbol{h}_k + \sigma_k^2\right), \tag{22}$$

$$\bar{d}_k \coloneqq \ln\left(\sum_{i\in\mathbb{K}\setminus\{k\}} \mathbf{m}_l^H \bar{\mathbf{V}}_i \mathbf{m}_l + \sum_{j\in\mathbb{L}\setminus\{l\}} \boldsymbol{m}_l^H \bar{\boldsymbol{W}}_j \boldsymbol{m}_l + \rho_l^2\right). \tag{23}$$

Then, we come up with the following restrictive approximation problem with a convex feasible set:

$$\begin{aligned}\mathcal{P}_{\text{1-D}}\colon \max\ & \mathrm{GSEE}'\big(\{\alpha_k\}, \{\beta_{k,l}\}, \{\mathbf{V}_i\}, \{\boldsymbol{W}_j\}\big)\\ \text{s.t.}\ & e^{\bar{a}_k}(a_k - \bar{a}_k + 1) \ge 2^{\alpha_k} - 1, && \text{(24a)}\\ & e^{\bar{b}_k}\big(b_k - \bar{b}_k + 1\big) \ge \sum_{i\in\mathbb{K}\setminus\{k\}} \mathbf{h}_k^H \mathbf{V}_i \mathbf{h}_k + \sum_{l=1}^{L} \boldsymbol{h}_k^H \boldsymbol{W}_l \boldsymbol{h}_k + \sigma_k^2, && \text{(24b)}\\ & e^{\bar{c}_{k,l} + \bar{d}_{k,l}}\big(c_{k,l} + d_{k,l} - \bar{c}_{k,l} - \bar{d}_{k,l} + 1\big) \ge \mathbf{m}_l^H \mathbf{V}_k \mathbf{m}_l, && \text{(24c)}\\ & \text{(16a), (16b), (15c), (15d), (21a), (21e), (21f).}\end{aligned}$$

Problem $\mathcal{P}_{\text{1-D}}$ can be solved by using the Dinkelbach method due to the following lemma.

Lemma 1 [40]: Let

$$F(\lambda) \coloneqq \left(\sum_{l=1}^{L}\sum_{k=1}^{K} \alpha_k - \beta_{k,l}\right) - \lambda P_{\mathrm{T}}\big(\{\mathbf{V}_i\}, \{\boldsymbol{W}_j\}\big)$$

where $\lambda \ge 0$. The optimal solution to $\mathcal{P}_{\text{1-D}}$ is obtained if and only if $F(\lambda) = 0$.

Algorithm 1 Dinkelbach Method Based Algorithm for Solving Problem $\mathcal{P}_{1\text{-D}}$

1: **Given** initial $\lambda[1]=0$, $\{\bar{a}_i\},\{\bar{b}_i\},\{\bar{c}_{i,j}\},\{\bar{d}_{i,j}\}$, and ε.
2: Set $q=0$.
3: **repeat**
4: $q=q+1$;
5: Obtain $\{\widehat{\mathbf{V}}_i[q]\}$, $\{\widehat{\boldsymbol{W}}_j[q]\}$, $\{\hat{\alpha}_i[q],\hat{a}_i[q],\hat{b}_i[q]\}$, and $\{\hat{\beta}_{i,j}[q],\hat{c}_{i,j}[q],\hat{d}_{i,j}[q]\}$ by solving $\mathcal{P}_2$;
6: Update $F(\lambda[q])=\sum_{l=1}^{L}\sum_{k=1}^{K}\big(\hat{\alpha}_k[q]-\hat{\beta}_{k,l}[q]\big)-\lambda[q]P_{\mathrm{T}}\big(\{\widehat{\mathbf{V}}_i[q]\},\{\widehat{\boldsymbol{W}}_j[q]\}\big)$;
7: Update $\lambda[q+1]=\frac{\sum_{l=1}^{L}\sum_{k=1}^{K}\big(\hat{\alpha}_k[q]-\hat{\beta}_{k,l}[q]\big)}{P_{\mathrm{T}}\big(\{\widehat{\mathbf{V}}_i[q]\},\{\widehat{\boldsymbol{W}}_j[q]\}\big)}$;
8: **until** $F(\lambda[q])<\varepsilon$.
9: **Output** $\{\mathbf{V}_i[q]\},\{\boldsymbol{W}_j[q]\},\{a_i[q],b_i[q]\},\{c_{i,j}[q],d_{i,j}[q]\}$.

Because $F(\lambda)$ is concave when λ is fixed, the Dinkelbach method can be employed to iteratively solve the following convex problem:

$$\mathcal{P}_2:\ \max\ F(\lambda)\quad \text{s.t.}\ \ (16\text{a}),\ (16\text{b}),\ (15\text{c}),\ (15\text{d}),\ (21\text{a}),\ (21\text{e}),\ (21\text{f}),\ (24\text{a}),\ (24\text{b}),\ (24\text{c})$$

until $F(\lambda)=0$, where the feasible set of $\mathcal{P}_2$ is identical to that of $\mathcal{P}_{1\text{-D}}$. Algorithm 1 for solving $\mathcal{P}_{1\text{-D}}$ is proposed to implement this method, which updates the optimal $F(\lambda[q])$ by solving $\mathcal{P}_2$ at the iteration q. This algorithm can yield an optimal solution to $\mathcal{P}_{1\text{-D}}$ because $F(\lambda[q])$ monotonically decreases with q until $F(\lambda[q])<\varepsilon$ where $\varepsilon>0$ is the pre-assigned convergence tolerance [31]. It is noticeable that $\lambda[q]$ is actually the GSEE$'$ achieved when Algorithm 1 converges, under the premise that the parameters $\{\bar{a}_i\}$, $\{\bar{b}_i\}$, $\{\bar{c}_{i,j}\}$, and $\{\bar{d}_{i,j}\}$ are given.

Now we are at the final stage to design our GSEEM algorithm for handling $\mathcal{P}_1$. The SCA based approach is implemented by Algorithm 2, that successively solves $\mathcal{P}_{1\text{-D}}$ using Algorithm 1 until convergence, and the obtained solution $\{\widehat{\mathbf{V}}_i[t]\}$ and $\{\widehat{\boldsymbol{W}}_j[t]\}$ to $\mathcal{P}_{1\text{-C}}$ is then further used to find the desired solution $\{\mathbf{v}_i[t]\}$ and $\{\boldsymbol{w}_j[t]\}$ to problem $\mathcal{P}_1$ through either rank-one decomposition or Gaussian randomization. Note that $\{\widehat{\mathbf{V}}_i[t]\}$ and $\{\widehat{\boldsymbol{W}}_j[t]\}$ can be shown to be a KKT point of $\mathcal{P}_{1\text{-C}}$ as stated in the following proposition.

Proposition 1: The sequence $\{\widehat{\mathbf{V}}_k[t],\widehat{\boldsymbol{W}}_l[t]\}$ yielded by Algorithm 2 (prior to Step 8, rank-one approximation) converges to a KKT point of $\mathcal{P}_{1\text{-C}}$.

Proof: See the Appendix.

B. Computational Complexity Analysis

For Algorithm 2, there are two iteration loops, where the outer iteration loop is based on SCA and the inner iteration loop is based on Dinkelbach method. In each iteration, the problem required to be solved is in fact convex problem $\mathcal{P}_2$. However, we need to convert the complex-valued problem $\mathcal{P}_2$ into the equivalent real-valued problem before analyzing the computational complexity [33] of Algorithm 2. For the sake of simplicity, let us assume that the decision variables in $\mathcal{P}_2$ are real-valued. Since the constraints of $\mathcal{P}_2$ only involve linear matrix inequality (LMI), $\mathcal{P}_2$ can be solved by using the standard interior-point method, and the corresponding computational complexity can be calculated by the following steps [41, Lecture 6], [42]. In $\mathcal{P}_2$, there are K matrix variables of size N_{p}, L matrix variables of size N_{s}, and $(3K+3KL)$ variables. Thus, the number of decision variables $\tilde{n}_1$ is $(KN_{\mathrm{p}}^2+LN_{\mathrm{s}}^2+3K+3KL)$. Besides, problem $\mathcal{P}_2$ contains $Z=(3KL+4K+L+1)$ LMI constraints of size 1, K LMI constraints of size N_{p} and L LMI constraints of size N_{s}. Thus, the computational complexity of Algorithm 2 is given by

$$\mathcal{O}\Bigg(\tilde{m}_1\tilde{q}_1\tilde{n}_1\ln(1/\tilde{\varepsilon})\sqrt{\big(KN_{\mathrm{p}}+LN_{\mathrm{s}}+Z\big)}\Big((\tilde{n}_1+1)Z+KN_{\mathrm{p}}^3+LN_{\mathrm{s}}^3+\tilde{n}_1\Big(KN_{\mathrm{p}}^2+LN_{\mathrm{s}}^2\Big)+\tilde{n}_1^2\Big)\Bigg).$$

where $\tilde{m}_1$ is the number of iterations spent by Algorithm 2, $\tilde{q}_1$ is that spent by Algorithm 1, provided that a $\tilde{\varepsilon}$-optimal solution is considered for $\mathcal{P}_2$.

Algorithm 2 SCA-Based Algorithm for Handling Problem $\mathcal{P}_{1\text{-C}}$

1: **Given** $\{\bar{a}_i,\bar{b}_i\},\{\bar{c}_{i,j},\bar{d}_{i,j}\}$ that are feasible to $\mathcal{P}_{1\text{-D}}$.
2: Set $t=0$.
3: **repeat**
4: $t=t+1$;
5: Obtain $\{\widehat{\mathbf{V}}_i[t]\},\{\widehat{\boldsymbol{W}}_j[t]\}$, $\{\hat{a}_i[t],\hat{b}_i[t]\}$, $\{\hat{c}_{i,j}[t],\hat{d}_{i,j}[t]\}$ by solving $\mathcal{P}_{1\text{-D}}$ using Algorithm 1;
6: Update $\bar{a}_k=\hat{a}_k[t]$, $\bar{b}_k=\hat{b}_k[t]$, $\forall k\in\mathbb{K}$, $\bar{c}_{k,l}=\hat{c}_{k,l}[t]$, $\bar{d}_{k,l}=\hat{d}_{k,l}[t]$, $\forall k\in\mathbb{K},\forall l\in\mathbb{L}$;
7: **until** the GSEE$'[t]$ convergence criterion is met.
8: Obtain $\{\mathbf{v}_i[t]\}$ and $\{\boldsymbol{w}_j[t]\}$ by rank-one decomposition if $\{\widehat{\mathbf{V}}_i[t]\}$ and $\{\widehat{\boldsymbol{W}}_j[t]\}$ (approximate solution to $\mathcal{P}_{1\text{-C}}$) are of rank one; otherwise perform Gaussian randomization to obtain a rank-one approximate solution to $\mathcal{P}_1$.
9: Obtain $\mathrm{GSEE}(\{\mathbf{v}_i[t]\},\{\boldsymbol{w}_j[t]\})$ by (9).
10: **Output** $\{\mathbf{v}_i[t]\}$, $\{\boldsymbol{w}_j[t]\}$, and $\mathrm{GSEE}(\{\mathbf{v}_i[t]\},\{\boldsymbol{w}_j[t]\})$.

C. Performance Analysis

Because the considered GSEEM problem $\mathcal{P}_1$ (see (11)) involves the secrecy rate and the power consumption in the objective function (see (9)). To provide more insights into the GSEE performance of the proposed GSEEM algorithm (Algorithm 2), we qualitatively compare $\mathcal{P}_1$ with the traditional SRM problem and PM problem based on empirical observations in this subsection.

The corresponding SRM problem (i.e., to maximize the numerator of GSEE) [34] and PM problem (i.e., to minimize the denominator of GSEE) [35] can be respectively expressed as follows.

$$\mathrm{SRM}:\ \max\ \mathcal{R}^{(\mathrm{Sec})}\big(\{\mathbf{v}_i\},\{\boldsymbol{w}_j\}\big)\quad \text{s.t.}\ \ (11\text{a}),\ (11\text{b}),\ (11\text{c}). \tag{25}$$

$$\mathrm{PM}:\ \min\ P_{\mathrm{T}}\big(\{\mathbf{v}_i\},\{\boldsymbol{w}_j\}\big)\quad \text{s.t.}\ \ (11\text{a}),\ (11\text{b}). \tag{26}$$

The performance behaviors of Algorithm 2 are discussed in the following remarks.

Remark 2 (Critical $P_{\rm actual}$): The obtained GSEE by Algorithm 2 increases with the total power consumption $P_{\rm T} = P_{\rm actual} + P_{\rm c}$ (see (1)) until a critical $P_{\rm actual}$ (see (2)), denoted as $P^{\star}_{\rm actual}$, is reached provided that $P_{\rm T} < P_{\max}$. If $P_{\max} > P^{\star}_{\rm actual} + P_{\rm c}$, the GSEE will no longer increase, meaning that the power exceeding $P^{\star}_{\rm actual} + P_{\rm c}$ is redundant. Therefore, the optimal GSEE and the associated $P^{\star}_{\rm actual}$ can be obtained by setting $P_{\max} = \infty$ for problem $\mathcal{P}_1$.

Remark 3 (Circuit Power): The GSEE performance (with the $P_{\rm actual} = P^{\star}_{\rm actual}$) of Algorithm 2 decreases with the circuit power $P_{\rm c}$ simply because $P_{\rm c}$ can only lower GSEE like AWGN to the system design, although both the associated sum of secrecy rates $\mathcal{R}^{(\rm sec)}$ (see (10), numerator of GSEE) and the total power consumption $P_{\rm T}$ (denominator of GSEE) increase with $P_{\rm c}$ in a consistent fashion for maximizing GSEE.

Remark 4 (Connection With SRM Design): The GSEE performance associated with the SRM design (see (25)) monotonically increases with $P_{\rm T} = P_{\max}$. It was empirically observed that the SRM design and Algorithm 2 share almost the same GSEE performance for $P_{\rm actual} \le P^{\star}_{\rm actual}$. Beyond $P^{\star}_{\rm actual}$, the SRM design in terms of GSEE performs worse for larger $P_{\max}$, although its $\mathcal{R}^{(\rm sec)}$ performance continues to improve.

Remark 5 (Connection With PM Design): We empirically found that the GSEE performance associated with the PM design increases with the QoS of PUs (provided that $\mathcal{Q}^{(\rm p)}_k = \mathcal{Q}^{(\rm p)}$ for all k for simplicity) before a critical $\mathcal{Q}^{(\rm p)}$, denoted as $\mathcal{Q}^{\star}$ is reached, and then decreases with $\mathcal{Q}^{(\rm p)}$ afterwards (i.e., over $\mathcal{Q}^{(\rm p)} > \mathcal{Q}^{\star}$). The GSEE of the PM design for $\mathcal{Q}^{(\rm p)} = \mathcal{Q}^{\star}$ turns out to be a good approximation to that of Algorithm 2 for $\mathcal{Q}^{(\rm p)} \le \mathcal{Q}^{\star}$, implying that the QoS requirement for Algorithm 2 can be upgraded as $\mathcal{Q}^{(\rm p)} = \mathcal{Q}^{\star}$. When $\mathcal{Q}^{(\rm p)} > \mathcal{Q}^{\star}$, they have almost the same GSEE performance, implying that the solution to the PM design for $\mathcal{Q}^{(\rm p)} \ge \mathcal{Q}^{\star}$ can be used as a surrogate to that of Algorithm 2. The reasons for the intriguing relation between Algorithm 2 and the PM design are as follows.

Suppose that the channel is feasible for Problem $\mathcal{P}_1$. Let $P_{\rm actual}$ and γ denote the optimal transmission power and the associated GSEE of the PM design, respectively. A characteristic of $R^{(\rm p)}_k$ (see (4)) is that $R^{(\rm p)}_k \approx \log_2(1+\xi_k\|\mathbf{v}_k\|^2)$ (where $\xi_k > 0$) is a concave function that increases with $\|\mathbf{v}_k\|^2$, and its slope $\xi_k/(1+\xi_k\|\mathbf{v}_k\|^2) > 0$ is smaller for larger $\|\mathbf{v}_k\|^2$. Then, the resulting $\min_k\{R^{(\rm p)}_k\} = \mathcal{Q}^{(\rm p)}$ (see (11a)) for the PM design implies that $\mathcal{R}^{(\rm Sec)}$ (see (10)) increases with $\mathcal{Q}^{(\rm p)}$. Therefore, $\gamma = \mathcal{R}^{(\rm Sec)}/(P_{\rm actual}+P_{\rm c})$ increases with $\mathcal{Q}^{(\rm p)}$ until its peak is achieved for $\mathcal{Q}^{(\rm p)} = \mathcal{Q}^{\star}$, and then γ decreases for $\mathcal{Q}^{(\rm p)} > \mathcal{Q}^{\star}$, which accounts for the single lobe behavior of γ. Furthermore, for $\mathcal{Q}^{(\rm p)} > \mathcal{Q}^{\star}$, the resulting values of $\mathcal{R}^{(\rm Sec)}$ for both the PM design and Algorithm 2 are dominated by $\mathcal{Q}^{(\rm p)}$, and meanwhile their GSEE performance gap is smaller for larger $\mathcal{Q}^{(\rm p)}$ (i.e., the term $R^{(\rm Eve)}_{k,l}$ (see (7)) in $\mathcal{R}^{(\rm Sec)}$ is negligible). In other words, their GSEE performances are close to each other over the region $\mathcal{Q}^{(\rm p)} > \mathcal{Q}^{\star}$.

IV. The PMBSS Algorithm

Based on the preceding analyses in Remark 5, the performance of Algorithm 2 can be predicted from the PM design results, because the computation complexity of the latter is significantly smaller than the former. Hence, to search for a proper QoS, denoted as $\mathcal{Q}^{\star}$, such that the achieved GSEE$'$ yielded by the PM design (with QoS selected from $\{\mathcal{Q}^{\star}, \mathcal{Q}^{(\rm p)}\}$) is comparable to (though lower than) that yielded by Algorithm 2, the following 2-step searching scheme is proposed:

Searching Scheme (PMBSS):

(*S1*) Obtain $\mathcal{Q}^{\star}$ and the associated beamforming solution and GSEE$'$ of the PM design.

(*S2*) If $\mathcal{Q}^{\star} > \mathcal{Q}^{(\rm p)}$, then the results obtained in *(S1)* are the predicted solution and GSEE$'$ of Algorithm 2; otherwise, with $\mathcal{Q}^{(\rm p)}$ as the target QoS, obtain the beamforming solution and GSEE$'$ of the PM design as the predicted solution and GSEE$'$ of Algorithm 2.

In (*S1*), a widely used golden search method [36] can be applied to efficiently find $\mathcal{Q}^{\star}$ since the GSEE$'$ associated with the PM design is unimodal with respect to $\mathcal{Q}^{(\rm p)}$ based on extensive simulation results. Moreover, we solve the following SDR of problem (26):

$$\begin{aligned} \mathrm{PM}_{(\mathrm{SDR})}: \ \min \ & P_{\rm T}\big(\{\mathbf{V}_i\}, \{\boldsymbol{W}_j\}\big) \\ \text{s.t.} \ & R^{(\rm p)}_k\big(\{\mathbf{V}_i\}, \{\boldsymbol{W}_j\}\big) \ge q^{(\rm p)}, \\ & R^{(\rm s)}_l\big(\{\mathbf{V}_i\}, \{\boldsymbol{W}_j\}\big) \ge \mathcal{Q}^{(\rm s)}, \\ & \mathbf{V}_k \succeq \mathbf{0},\ \boldsymbol{W}_l \succeq \mathbf{0},\ \forall k \in \mathbb{K},\ \forall l \in \mathbb{L}, \end{aligned} \tag{27}$$

provided that all the target rates for the PUs (SUs) are identical to $q^{(\rm p)}$ ($\mathcal{Q}^{(\rm s)}$). Note that $\mathrm{PM}_{(\mathrm{SDR})}$ can be easily reformulated into a convex problem, and thus can be solved optimally using any off-the-shelf convex servers. Thus, the resulting PMBSS algorithm (Algorithm 3) is proposed, which yields $\mathcal{Q}^{\star}$ and the predicted solution for Algorithm 2, for a given $\mathcal{Q}^{(\rm p)}$ and $q^{(\rm p)}_{\max}$ (upper bound of $q^{(\rm p)}$) and the preassigned convergence tolerance δ. A suitable choice for $q^{(\rm p)}_{\max}$ is needed because if the main lobe width of the GSEE$'$ may be significantly smaller than $q^{(\rm p)}_{\max}$, the golden section search may fail. The reason for this is that both $\mathrm{GSEE}'(\{\widehat{\mathbf{V}}_i\}, \{\widehat{\boldsymbol{W}}_j\})$ and $\mathrm{GSEE}'(\{\widetilde{\mathbf{V}}_i\}, \{\widetilde{\boldsymbol{W}}_j\})$ may happen numerically to be zero in Step 7 such that the loop (Step 3 through Step 11) in Algorithm 3 will end up with $\mathcal{Q}^{\star} \approx q^{(\rm p)}_{\max}$ for which the associated GSEE$'$ is numerically zero. One can overcome this issue using the bisection method, i.e., successively updating $q^{(\rm p)}_{\max}$ by $q^{(\rm p)}_{\max}/2$ until $\mathcal{Q}^{\star}$ (for which the associated GSEE$'$ is numerically greater than zero) is obtained by Algorithm 3.

Supposing that $\mathrm{GSEE(Alg2)}_i$ and $\mathrm{GSEE(PMBSS)}_i$ respectively stand for the GSEE associated with Algorithm 2 and the proposed PMBSS for the *i*-th channel realization, the searching accuracy is defined as

$$\eta := \frac{\sum_{i=1}^{M} \mathrm{GSEE(PMBSS)}_i}{\sum_{i=1}^{M} \mathrm{GSEE(Alg2)}_i} \tag{28}$$

where M is the number of feasible channel realizations. The larger η, the better the searching accuracy of the PMBSS.

Algorithm 3 Algorithm for Implementing the PMBSS

1: **Given** $q_{\max}^{(\mathrm{p})}$, $\mathcal{Q}^{(\mathrm{p})}$ and convergence tolerance $\delta > 0$.
2: **Set** $r_1 \coloneqq 0$, $r_2 \coloneqq q_{\max}^{(\mathrm{p})}$, and $R_G \coloneqq \frac{\sqrt{5}-1}{2}$.
3: **repeat**
4: Set $r \coloneqq r_2 - r_1$;
5: Set $r_3 \coloneqq r_2 - R_G \times r$ and $r_4 \coloneqq r_1 + R_G \times r$;
6: Obtain $\{\widehat{\mathbf{V}}_i\}, \{\widehat{\boldsymbol{W}}_j\}$ and $\{\widetilde{\mathbf{V}}_i\}, \{\widetilde{\boldsymbol{W}}_j\}$ by solving (27) for $q^{(\mathrm{p})} = r_3$ and $q^{(\mathrm{p})} = r_4$, respectively;
7: Compute $\mathrm{GSEE}'(\{\widehat{\mathbf{V}}_i\}, \{\widehat{\boldsymbol{W}}_j\})$ and $\mathrm{GSEE}'(\{\widetilde{\mathbf{V}}_i\}, \{\widetilde{\boldsymbol{W}}_j\})$ by (17);
8: **If** $\mathrm{GSEE}'(\{\widehat{\mathbf{V}}_i\}, \{\widehat{\boldsymbol{W}}_j\}) > \mathrm{GSEE}'(\{\widetilde{\mathbf{V}}_i\}, \{\widetilde{\boldsymbol{W}}_j\})$, update $r_2 \coloneqq r_4$,
9: **else** update $r_1 \coloneqq r_3$;
10: **until** $|r_2 - r_1| < \delta(|r_3| + |r_4|)$.
11: **Set** $\mathcal{Q}^{\star} = \frac{r_1 + r_2}{2}$.
12: **If** $\mathcal{Q}^{\star} > \mathcal{Q}^{(\mathrm{p})}$, obtain $\{\mathbf{V}_i{}^{\star}\}$ and $\{\boldsymbol{W}_j{}^{\star}\}$ by solving (27) for $q^{(\mathrm{p})} = \mathcal{Q}^{\star}$; otherwise solve (27) for $q^{(\mathrm{p})} = \mathcal{Q}^{(\mathrm{p})}$ to obtain $\{\mathbf{V}_i{}^{\star}\}$ and $\{\boldsymbol{W}_j{}^{\star}\}$.
13: Obtain $\{\mathbf{v}_i{}^{\star}\}$ and $\{\boldsymbol{w}_j{}^{\star}\}$ by rank-one decomposition if $\{\mathbf{V}_i{}^{\star}\}$ and $\{\boldsymbol{W}_j{}^{\star}\}$ are of rank one; otherwise perform Gaussian randomization to obtain a rank-one approximate solution.
14: Obtain $\mathrm{GSEE}(\{\mathbf{v}_i{}^{\star}\}, \{\boldsymbol{w}_j{}^{\star}\})$ by (9).
15: **Output** $\{\mathbf{v}_i{}^{\star}\}$, $\{\boldsymbol{w}_j{}^{\star}\}$, $\mathcal{Q}^{\star}$, and $\mathrm{GSEE}(\{\mathbf{v}_i{}^{\star}\}, \{\boldsymbol{w}_j{}^{\star}\})$.

Surely, the obtained solution can also be used as the initial condition for Algorithm 2 for faster convergence.

V. Simulation Results

In this section, we present some simulation results to demonstrate the performance of the proposed GSEEM algorithm (Algorithm 2) and Algorithm 3. The simulation setting is as follows: $K \in \{1, 2, 3\}$ and $L \in \{1, 2, 3, 5, 8, 10\}$ (number of PUs and number of SUs), $N_{\mathrm{p}} = N_{\mathrm{s}} = \mathcal{N} \in \{4, 6, 8, 12, 14\}$ (number of PTx antennas and number of STx antennas), $\mathcal{Q}_k^{(\mathrm{p})} = \mathcal{Q}^{(\mathrm{p})}$ (QoS of PUs), $\mathcal{Q}_l^{(\mathrm{s})} = \mathcal{Q}^{(\mathrm{s})}$ (QoS of SUs), and ${\sigma_k}^2 = {\rho_l}^2 = 0.01$ for all k and l. Five hundred independent channel realizations for $\{\mathbf{h}_k, \boldsymbol{h}_k\}$ and $\{\mathbf{m}_l, \boldsymbol{m}_l\}$ are spatially independent identically distributed (i.i.d.) and have standard circularly symmetric complex Gaussian distributions, i.e., $\mathcal{CN}(\mathbf{0}, \mathbf{C})$, where $\mathbf{C}$ denotes the covariance matrix. All the involved convex formulations are solved using the convex solver `SeDuMi` [43], [44] under Mathworks MATLAB R2019a and running on a computer with Core-i5-4460K CPU (3.2 GHz CPU speed) and with 8 GB RAM.

A. Simulation Results for i.i.d. Channels ($\boldsymbol{C} = \boldsymbol{I}_{\mathcal{N}}$)

Because $\mathcal{P}_{1\text{-C}}$ may be infeasible for a given channel realization, we first investigate the feasibility rate for handling $\mathcal{P}_{1\text{-C}}$ by the proposed GSEEM algorithm, over the generated 500 channel realizations. The obtained results for the feasibility rate are displayed in Fig. 3. It is observed that

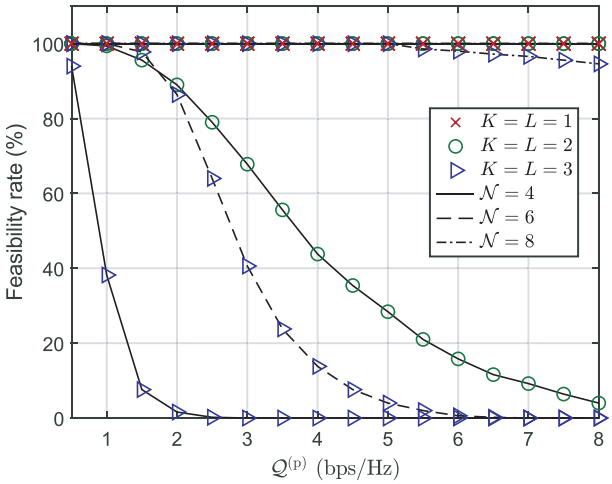

Fig. 3. Feasibility rates (%) versus $\mathcal{Q}^{(\mathrm{p})}$, for $K = L \in \{1, 2, 3\}$, where $\mathcal{N} \in \{4, 6, 8\}$, $P_{\max} = \infty$, $P_{\mathrm{c}} = 0.1$ W, and $\mathcal{Q}^{(\mathrm{s})} = 1$ bps/Hz.

for $K = L = 1$, the considered problem is always feasible. However, for $K = L = 2$, 3, feasibility rate decreases with $\mathcal{Q}^{(\mathrm{p})}$ due to the inadequate spatial DoF at the PTx and STx. As mentioned in Section III, when the designed $\widehat{\mathbf{V}}_i$ and $\widehat{\boldsymbol{W}}_j$ are not rank-one, Gaussian randomization is employed to recover the approximate rank-one solutions. Hence, the designed $(\{\widehat{\mathbf{V}}_i\}, \{\widehat{\mathbf{W}}_j\})$ is considered to be of rank one if

$$\frac{\lambda_{\max}\left(\widehat{\mathbf{V}}_i\right)}{\mathrm{Tr}\left(\widehat{\mathbf{V}}_i\right)} \geq 0.999, \quad \frac{\lambda_{\max}\left(\widehat{\mathbf{W}}_j\right)}{\mathrm{Tr}\left(\widehat{\mathbf{W}}_j\right)} \geq 0.999. \tag{29}$$

In our simulation, all the feasible solutions are rank one matrices without need of rank-one approximation. This indicates that if spatial DoF is sufficient (namely sufficient antennas), the solution obtained by Algorithm 2 is always of rank one; otherwise, the GSEE problem is infeasible, implying that spatial DoF is the key resource instead of the total power consumption.

Figure 4 shows the histogram of GSEE and that of $P_{\mathrm{actual}}^{\star}$ obtained using Algorithm 2 over the generated feasible channel realizations. The mean and standard deviation of GSEE (see Fig. 4 (a)) are 35.9 bits/Hz/J and 17.2 bits/Hz/J, respectively, and those of $P_{\mathrm{actual}}^{\star}$ (see Fig. 4 (b)) are 0.32 W and 1.82 W, respectively. Note that the distribution of GSEE is approximately Gaussian, while the distribution of $P_{\mathrm{actual}}^{\star}$ is approximately Rayleigh with a small standard deviation, i.e., quite concentrates in the vicinity of its mean value, thus consistent with Remark 2 since $P_{\mathrm{actual}}^{\star}$ depending on the channel is obtained with $P_{\max} = \infty$ to achieve the maximum GSEE performance by Algorithm 2.

Figure 5 shows the convergence behavior of the proposed algorithm for a typical feasible channel realization, where q and t denote the iteration numbers of Algorithm 1 and Algorithm 2, respectively. One can see that both optimal $F(\lambda[q])$ (left plot) yielded by the former and $\mathrm{GSEE}'[t]$ (right plot) yielded by the latter converge fast and monotonically to zero and to 38.8 bits/Hz/J, respectively. These

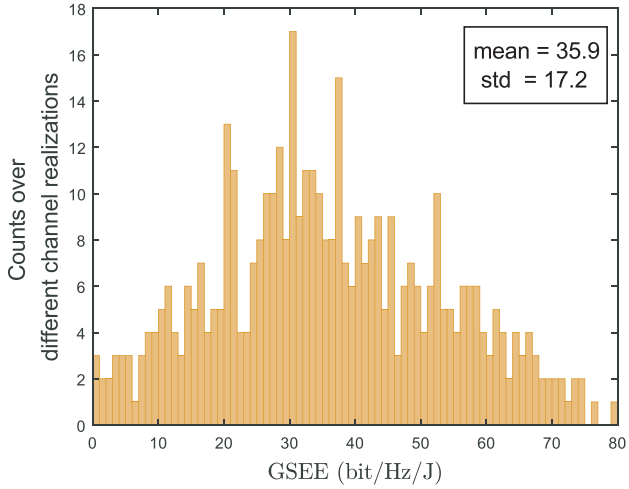

Fig. 4. Histograms of (a) GSEE, and (b) $P^{\star}_{\text{actual}}$ of the obtained simulation results over the generated feasible channel realizations by Algorithm 2 for $K = L = 2$, $\mathcal{N} = 4$, $P_{\max} = \infty$, $P_{\text{c}} = 0.1$ W, $\mathcal{Q}^{(\text{p})} = 2$ bps/Hz, and $\mathcal{Q}^{(\text{s})} = 1$ bps/Hz.

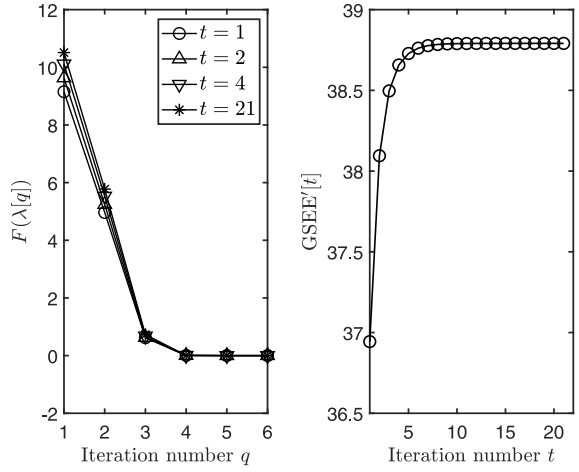

Fig. 5. Optimal $F(\lambda[q])$ versus q (left plot) obtained by Algorithm 1, for iterations $t = 1$, $t = 2$, $t = 4$ and $t = 21$ of Algorithm 2, and GSEE$'[t]$ versus t (right plot) obtained by Algorithm 2 for a typical feasible channel realization for $K = L = 2$, $\mathcal{N} = 4$, $P_{\max} = \infty$, $P_{\text{c}} = 0.1$ W, $\mathcal{Q}^{(\text{p})} = 2$ bps/Hz, and $\mathcal{Q}^{(\text{s})} = 1$ bps/Hz.

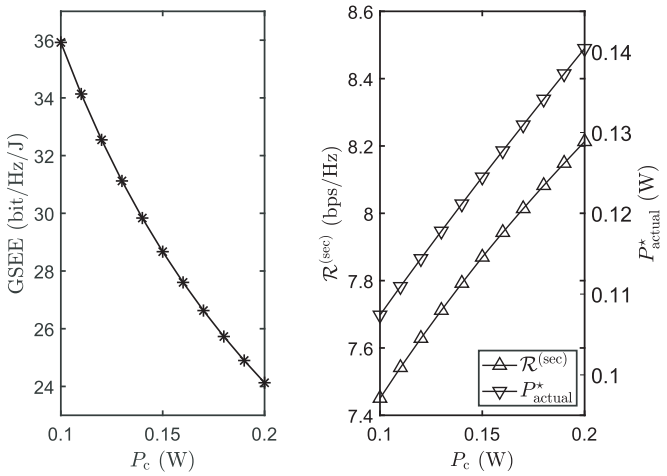

Fig. 6. The averaged GSEE (left plot), as well as averaged $\mathcal{R}^{(\text{Sec})}$ and $P^{\star}_{\text{actual}}$ (right plot) obtained by Algorithm 2 with respect to P_{c} over the generated feasible channel realizations for $K = L = 2$, $\mathcal{N} = 4$, $P_{\max} = \infty$, $\mathcal{Q}^{(\text{p})} = 2$ bps/Hz, and $\mathcal{Q}^{(\text{s})} = 1$ bps/Hz.

results also account for the anticipated convergence behavior of Dinkelbach method based Algorithm 1 and SCA-based Algorithm 2.

Figure 6 shows the averaged GSEE, $\mathcal{R}^{(\text{Sec})}$ and $P^{\star}_{\text{actual}}$ versus P_{c} yielded by Algorithm 2 over the generated feasible channel realizations. It can be seen from this figure that GSEE decreases with P_{c} (left plot), whereas $\mathcal{R}^{(\text{Sec})}$ and $P^{\star}_{\text{actual}}$ increase with P_{c} (right plot). These results are consistent with Remark 3.

Figure 7 shows GSEEs with respect to $P_{\max}$ (left plot) obtained by Algorithm 2 (solid curves) and the SRM design (dashed curves) for a typical feasible channel realization. From the left plot, one can see that Algorithm 2 and the SRM design (see (25)) have the same performance for $P_{\max} \leq 0.208$ W (i.e., $P^{\star}_{\text{actual}} = 0.208 - 0.1 = 0.108$ W due to $P_{\text{c}} = 0.1$ W), while the former maintains the same GSEE performance for $P_{\max} \geq 0.208$ W, but the latter performs worse for larger $P_{\max}$. These results are consistent with Remark 4. On the other hand, the corresponding result for P_{actual} with respect to $P_{\max}$ for the same realization is displayed in the right plot of Fig. 7, again, showing that $P_{\text{actual}} = P_{\max} - P_{\text{c}}$ for all $P_{\max}$ (blue dashed curve) associated with the SRM design, and this is also true for $P_{\max} \leq 0.208$ (red solid curve) associated with Algorithm 2. However, P_{actual} for Algorithm 2 remains unchanged when $P_{\max} \geq 0.208$ W (as indicated by circles).

Figure 8 shows GSEEs (left plot) and P_{actual} (right plot) with respect to $\mathcal{Q}^{(\text{p})}$ obtained by Algorithm 2 (solid curves) and the PM design (dashed curves) for a typical feasible channel realization, respectively. From the left plot, one can see that they have comparable performance for $\mathcal{Q}^{(\text{p})} \geq 2.75$ bps/Hz (which is larger than the required $\mathcal{Q}^{(\text{p})} = 2$ bps/Hz), whereas for $\mathcal{Q}^{(\text{p})} \leq 2.75$ bps/Hz, Algorithm 2 has better GSEEs performance (approximately a constant GSEE). In other words, $\mathcal{Q}^{\star} = 2.75$ bps/Hz. These results are consistent with Remark 5. Furthermore, note that $P_{\text{actual}} = 0.082$ W (indicated by a circle in the right plot) associated with the PM design for $\mathcal{Q}^{(\text{p})} = \mathcal{Q}^{\star}$, and it is closely approximating to

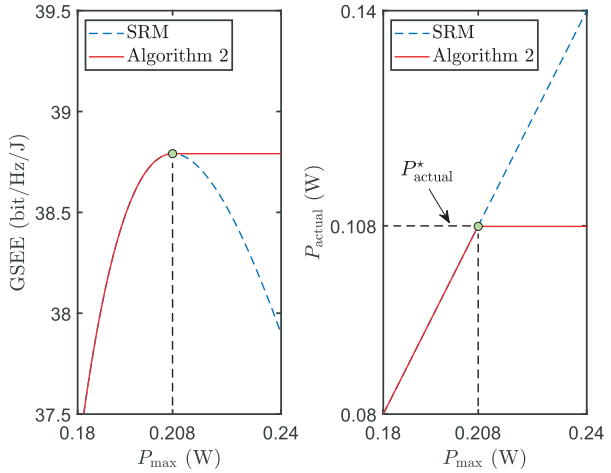

Fig. 7. GSEE performance (left plot) and P_{actual} performance (right plot) with respect to $P_{\max}$, obtained by Algorithm 2 and the SRM design for a typical feasible channel realization for $K = L = 2$, $\mathcal{N} = 4$, $P_{\text{c}} = 0.1$ W, $\mathcal{Q}^{(\text{p})} = 2$ bps/Hz, and $\mathcal{Q}^{(\text{s})} = 1$ bps/Hz.

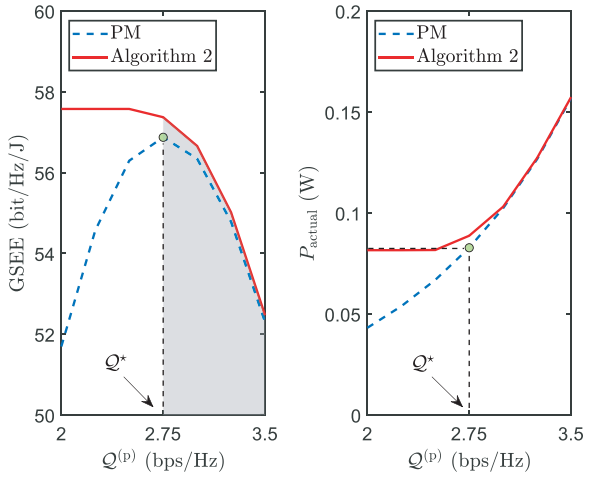

Fig. 8. GSEE performance (left plot) and P_{actual} performance (right plot) with respect to $\mathcal{Q}^{(\text{p})}$, obtained by Algorithm 2 and the PM design for a typical feasible channel realization for $K = L = 2$, $\mathcal{N} = 4$, $P_{\max} = \infty$, $P_{\text{c}} = 0.1$ W and $\mathcal{Q}^{(\text{s})} = 1$ bps/Hz, where, in the right plot, P_{actual} denotes the optimal value for the PM design and $P_{\text{actual}} = P^{\star}_{\text{actual}}$ for Algorithm 2.

$P^{\star}_{\text{actual}}$ yielded by Algorithm 2 as long as $\mathcal{Q}^{(\text{p})} \leq \mathcal{Q}^{\star}$. So the QoS requirement in the system design can be elevated to $\mathcal{Q}^{\star}$ for nearly the same GSEE performance that Algorithm 2 can achieve.

On the other hand, the averaged computation time per realization over all the feasible channel realizations for Algorithm 2 is 23.8 secs, while that for the PM design is 0.34 secs. Moreover, Fig. 9 shows the histogram of $\mathcal{Q}^{\star}$ yielded by the PM design, from which one can see that it is approximately Gaussian with around 39.4% of realizations for $\mathcal{Q}^{\star} > 2$ bps/Hz and the system QoS requirement of $\mathcal{Q}^{(\text{p})} = 2$ bps/Hz can be increased to $\mathcal{Q}^{\star}$ for such channel realizations. The resulting searching accuracy is $\eta = 95.85\%$ (see (28)) is achieved in the preceding simulation, showing the good searching accuracy of the PMBSS.

Next, let us show some simulation results for $K = L \in \{1, 2, 3\}$ and $\mathcal{N} = 4, 8$, which are displayed in Fig. 10, where

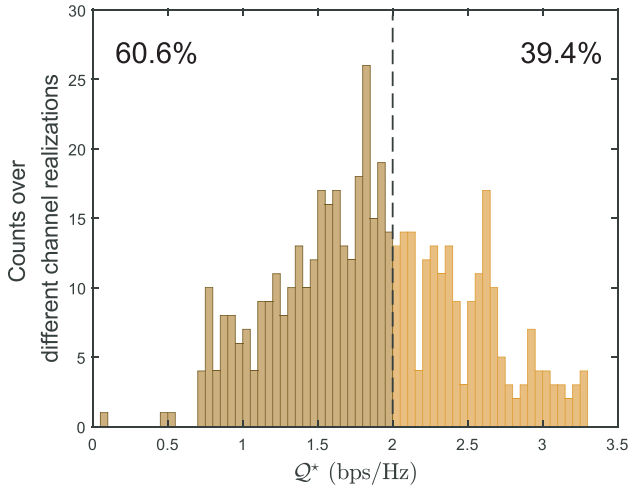

Fig. 9. Histogram of critical $\mathcal{Q}^{\star}$ of the obtained simulation results over the generated feasible channel realizations by the PM design for $K = L = 2$, $\mathcal{N} = 4$, $P_{\max} = \infty$, $P_{\text{c}} = 0.1$ W, and $\mathcal{Q}^{(\text{s})} = 1$ bps/Hz.

the yielded solution by PMBSS (Algorithm 3) is used to initialize Algorithm 2. From Fig. 10 (a), one can see that the average GSEE performances of Algorithm 2 and the searching scheme PMBSS are worse for larger $\mathcal{Q}^{(\text{p})}$ due to inadequate spatial DoF ($\mathcal{N} = 4$). However, the corresponding results for $K = L = 3$ are not shown in this figure due to too few feasible channel realizations available in average GSEE calculations (see Fig. 3), thus losing statistical reliability. As expected, the performance of the PMBSS is quite close to that of Algorithm 2 for $K = L = 2$, justifying high searching accuracy of PMBSS, while the searching accuracy of PMBSS for $K = L = 1$ is lower than for $K = L > 1$. The reason for this case is that the eavesdropper's achievable rate $R^{(\text{Eve})}_{k,l}$ (see (7), (8)) can be significantly suppressed by Algorithm 2, thereby leading to GSEE (see (9)) much larger than the corresponding GSEE yielded by Algorithm 3 thanks to sufficient spatial DoF. The corresponding simulation results for $\mathcal{N} = 8$ are shown in Fig. 10 (b). The above observations from Fig. 10 (a) also apply to Fig. 10 (b), in addition to the better GSEE performances for the two algorithms thanks to more spatial DoF for $\mathcal{N} = 8$ (without statistical unreliability). Moreover, an interesting characteristic of PMBSS is that the GSEE yielded by Algorithm 3 (dashed curve) is basically similar (in pattern) to that associated with the PM design for $\mathcal{Q}^{(\text{p})} > \mathcal{Q}^{\star}$ as shown in the shaded region in the left plot of Fig. 8, so is the GSEE associated with Algorithm 2 (solid curve) due to good searching accuracy of the searching scheme PMBSS.

On the other hand, the corresponding average running times for Algorithm 2 and Algorithm 3 are displayed in Fig. 10 (c) and Fig. 10 (d), for $\mathcal{N} = 4$ and $\mathcal{N} = 8$, respectively, showing that the running time for Algorithm 3 is much smaller than Algorithm 2 (around $3 \sim 5$ times and $4 \sim 10$ times smaller for $\mathcal{N} = 4$ and $\mathcal{N} = 8$, respectively).

Furthermore, we show some simulation results in Fig. 11, for $K = 2$, $L \in \{2, 5, 8, 10\}$ and $\mathcal{N} \in \{8, 12, 14\}$ for Algorithm 2. Specifically, larger numbers of SUs (eavesdroppers) than the number of PUs and larger antenna numbers

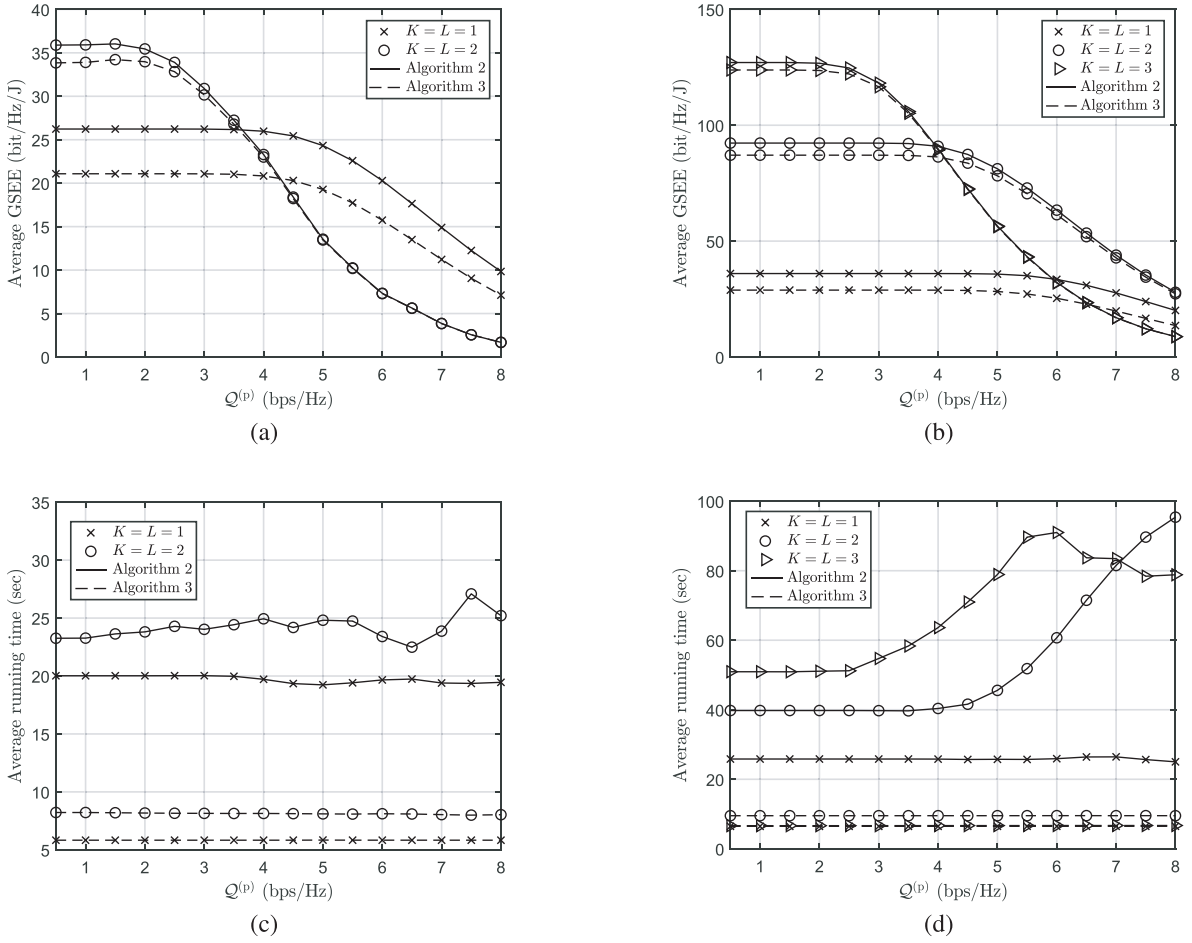

Fig. 10. Average GSEE performance for (a) $\mathcal{N} = 4$ and (b) $\mathcal{N} = 8$, and average running time with respect to $\mathcal{Q}^{(\mathrm{p})}$ for (c) $\mathcal{N} = 4$ and (d) $\mathcal{N} = 8$, obtained by Algorithm 2 and Algorithm 3 over the generated feasible channel realizations for $K = L \in \{1, 2, 3\}$, $P_{\max} = \infty$, $P_{\mathrm{c}} = 0.1$ W, and $\mathcal{Q}^{(\mathrm{s})} = 1$ bps/Hz.

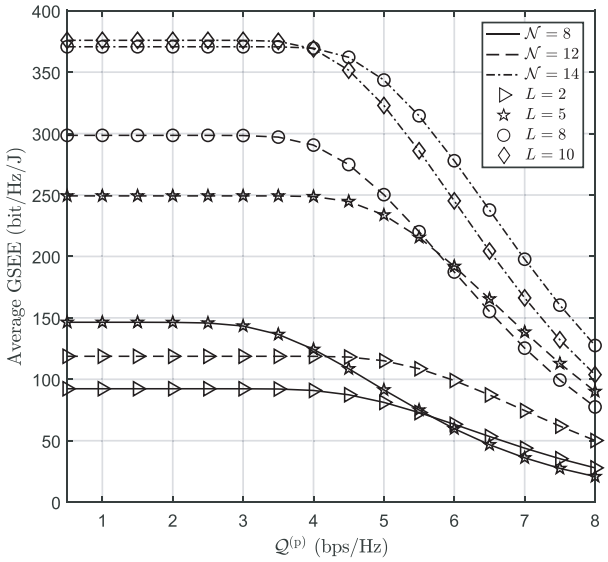

Fig. 11. Average GSEE performance with respect to $\mathcal{Q}^{(\mathrm{p})}$, obtained by Algorithm 2 over the generated feasible channel realizations for $K = 2$, $L \in \{2, 5, 8, 10\}$, $\mathcal{N} \in \{8, 12, 14\}$, $P_{\max} = \infty$, $P_{\mathrm{c}} = 0.1$ W, and $\mathcal{Q}^{(\mathrm{s})} = 1$ bps/Hz.

are considered in the results shown in this figure. All the observations about the GSEE performance of Algorithm 2 from Figs. 10 (a) and 10 (b) also apply to Fig. 11, demonstrating the good performance of Algorithm 2 because of sufficient spatial DoF provided for all the simulation cases. However, the crossover of its GSEE performance may occur for different L (see the curves for $L = 8$, $L = 10$ and $\mathcal{N} = 14$ (dash-dotted curves), $L = 5$, $L = 8$ and $\mathcal{N} = 12$ (dash curves), and $L = 2$, $L = 5$ and $\mathcal{N} = 8$ (solid curves). The reason for this could be that a threshold of $\mathcal{Q}^{(\mathrm{p})}$ (which is no less than $\mathcal{Q}^{\star}$) exists for which $P^{\star}_{\mathrm{actual}}$ increases faster for larger L when $\mathcal{Q}^{(\mathrm{p})} > \mathcal{Q}^{\star}$ in spite of more secrecy rates (each for a (PU, SU) pair) in the total secrecy rate $\mathcal{R}^{(\mathrm{sec})}$.

B. Simulation Results for Spatially Correlated Channels

This subsection shows some simulation results for the case of channels with strong spatial correlation, with the following covariance matrix given by [42]

$$[\mathbf{C}]_{ij} = 0.9^{|i-j|}. \tag{30}$$

Figures 12 (a) and 12 (b) for spatial correlation channels display the simulation results corresponding to Figs. 10 (a) and 10 (b) (for i.i.d. channels), respectively. One can see, from Figs. 12 (a) and 10 (a), ($K = L \in \{1, 2\}$, $\mathcal{N} = 4$) that all the observations for the latter also apply to the former, except for the better GSEE performance for the latter. This is also true for 12 (b) and 10 (b) ($K = L \in \{1, 2, 3\}$, $\mathcal{N} = 8$). These

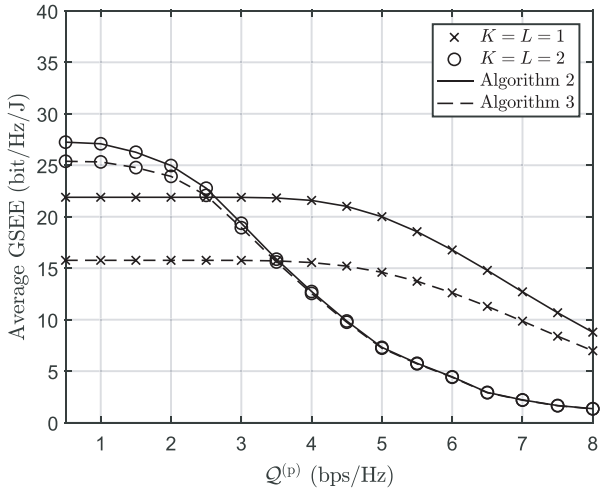

(a)

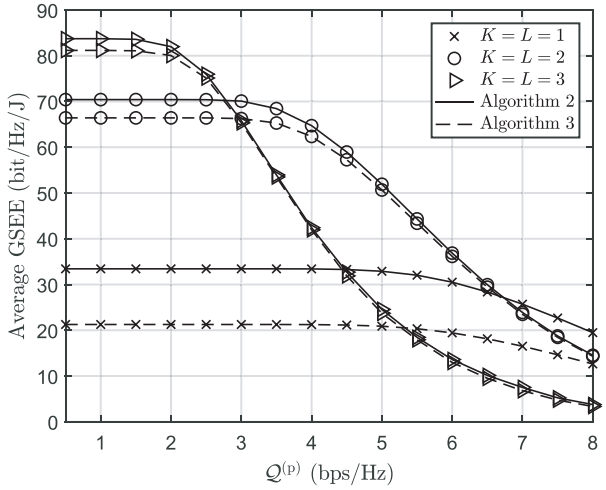

(b)

Fig. 12. Average GSEE performance for (a) $\mathcal{N} = 4$ and (b) $\mathcal{N} = 8$ with respect to $\mathcal{Q}^{(\mathrm{p})}$, obtained by Algorithm 2 and Algorithm 3 for spatial correlation channels (see (30)), where $K = L \in \{1, 2, 3\}$, $P_{\max} = \infty$, $P_{\mathrm{c}} = 0.1$ W, and $\mathcal{Q}^{(\mathrm{s})} = 1$ bps/Hz.

simulation results also justify the good performance of the proposed Algorithm 2 and Algorithm 3 for strong correlation channels, in spite of some GSEE performance loss compared with the case of i.i.d. channels.

VI. Conclusion

We have presented a secrecy energy efficient coordinated beamforming design for a multi-PU MISO USS-based CR networks in the presence of multiple untrusted SUs, which is implemented by the proposed GSEEM algorithm (Algorithm 2) through handling the non-convex GSEEM problem $\mathcal{P}_1$ (see (11)). The performance of Algorithm 2 was also analyzed, including algorithm convergence, computational complexity and the connection with the SRM design and the PM design. Inspired by the obtained analysis results, we further proposed the 2-step searching scheme (Algorithm 3) for efficiently finding an approximate solution to the considered GSEEM problem which is close to but worse than the one obtained by Algorithm 2. In other words, the designed beamforming vectors and the achieved GSEE performance using Algorithm 2 can also be efficiently predicted (with good accuracy) by Algorithm 3. Then, simulation results were presented to demonstrate the good performance of Algorithm 2 and Algorithm 3 as well as the validity of the analytical results (see Remark 2 through Remark 5). We would like to emphasize that the spatial DoF is the key factor to the GSEE performance. For given spatial DoF, the GSEE performance of Algorithm 2 mainly depends on the critical P_{actual} ($P^{\star}_{\mathrm{actual}}$, see Remark 2), and the maximally admissible QoS of the PUs $\mathcal{Q}^{(\mathrm{p})}$ for the same GSEE is actually the critical $\mathcal{Q}^{(\mathrm{p})}$ (i.e., $\mathcal{Q}^{\star}$) obtained by Algorithm 3 when $\mathcal{Q}^{(\mathrm{p})} < \mathcal{Q}^{\star}$, implying cost-free higher QoS benefit for PUs. However, if $\mathcal{Q}^{(\mathrm{p})} > \mathcal{Q}^{\star}$, it is necessary for the proposed GSEEM algorithm to increase DoF for maintaining or improving the achievable GSEE performance. In other words, $\mathcal{Q}^{\star}$ plays the role as the cutoff point of the GSEE performance of Algorithm 2 for the given DoF.

On the other hand, our simulation results also showed that the spatial DoF plays a crucial role to the GSEE performance of Algorithm 2, implying that the massive MIMO technology is potential to significantly upgrade the GSEE performance for CR networks, which is left as a future study. Moreover, if the CSI is only partially known or with some errors, then the corresponding robust beamforming design is also worthy of future study.

Appendix
Proof of Proposition 1

Let $\{\widehat{\mathbf{u}}[t]\} := \{\widehat{\mathbf{V}}_k[t], \widehat{\boldsymbol{W}}_l[t], \hat{\alpha}_k[t], \hat{\beta}_{k,l}[t], \hat{a}_k[t], \hat{b}_k[t], \hat{c}_{k,l}[t], \hat{d}_{k,l}[t]\}$ denote the optimal solution to $\mathcal{P}_{1\text{-D}}$ by Algorithm 1 at iteration t. Because the SCA is applied to handle $\mathcal{P}_{1\text{-C}}$, it is guaranteed that the optimal value $\mathrm{GSEE}'[t]$ is monotone increasing with respect to t and $\{\widehat{\mathbf{u}}[t]\}$ is feasible to both $\mathcal{P}_{1\text{-C}}$ and $\mathcal{P}_{1\text{-D}}$. Moreover, due to the total power constraint (11c), the sequence $\{\mathrm{GSEE}'[t]\}_{t=1}^{\infty}$ is bounded above, which implies the convergence of $\{\mathrm{GSEE}'[t]\}$.

Next, we show that $\{\widehat{\mathbf{u}}[t]\}$ converges to a KKT point of $\mathcal{P}_{1\text{-C}}$ as $t \to \infty$. For ease of later use, let us re-express the non-convex constraints (21b), (21c), (21d) of $\mathcal{P}_{1\text{-C}}$ as

$$f_1(\alpha_k, a_k) := 2^{\alpha_k} - 1 - e^{a_k} \le 0, \tag{31a}$$

$$f_2\Big(\{\mathbf{V}_i\}_{i\neq k}, \{\boldsymbol{W}_j\}, b_k\Big) := \sum_{i\in\mathbb{K}\setminus\{k\}} \mathbf{h}_k^H \mathbf{V}_i \mathbf{h}_k + \sum_{l=1}^{L} \boldsymbol{h}_k^H \boldsymbol{W}_l \boldsymbol{h}_k + \sigma_k^2 - e^{b_k} \le 0, \tag{31b}$$

$$f_3\big(\mathbf{V}_k, c_{k,l}, d_{k,l}\big) := \mathbf{m}_l^H \mathbf{V}_k \mathbf{m}_l - e^{c_{k,l}+d_{k,l}} \le 0. \tag{31c}$$

Then, the associated three convex constraints (24a), (24b), and (24c) of $\mathcal{P}_{1\text{-D}}$ at the iteration t can be re-expressed as

$$\bar{f}_1(\alpha_k, a_k | \hat{a}_k[t-1]) := 2^{\alpha_k} - 1 - e^{\hat{a}_k[t-1]}(a_k - \hat{a}_k[t-1] + 1) \le 0, \tag{32a}$$

$$\bar{f}_2\Big(\{\mathbf{V}_i\}_{i\neq k}, \{\boldsymbol{W}_j\}, b_k|\hat{b}_k[t-1]\Big) \coloneqq \sum_{i\in\mathbb{K}\setminus\{k\}} \mathbf{h}_k^H\mathbf{V}_i\mathbf{h}_k + \sum_{l=1}^{L} \boldsymbol{h}_k^H\boldsymbol{W}_l\boldsymbol{h}_k + \sigma_k^2 - e^{\hat{b}_k[t-1]}\Big(b_k - \hat{b}_k[t-1]+1\Big) \leq 0, \tag{32b}$$

$$\bar{f}_3\Big(\mathbf{V}_k, c_{k,l}, d_{k,l}|\hat{c}_{k,l}[t-1], \hat{d}_{k,l}[t-1]\Big) \coloneqq \mathbf{m}_l^H\mathbf{V}_k\mathbf{m}_l - e^{\hat{c}_{k,l}[t-1]+\hat{d}_{k,l}[t-1]} \times \Big((c_{k,l}+d_{k,l}) - \Big(\hat{c}_{k,l}[t-1]+\hat{d}_{k,l}[t-1]\Big)+1\Big) \leq 0, \quad \forall k\in\mathbb{K}, \quad \forall l\in\mathbb{L}. \tag{32c}$$

Let $\mathcal{L}(\{\widehat{\mathbf{u}}[t]\}, \boldsymbol{\lambda}[t])$ denote the Lagrangian of $\mathcal{P}_{1\text{-D}}$, where

$$\boldsymbol{\lambda}[t] \coloneqq \Big(\Big\{\lambda_k^a[t]\Big\}, \Big\{\lambda_l^b[t]\Big\}, \{\lambda^c[t]\}, \Big\{\lambda_k^d[t]\Big\}, \Big\{\lambda_{k,l}^e[t]\Big\}, \Big\{\lambda_{k,l}^f[t]\Big\}, \{\lambda_k^g[t]\}, \Big\{\lambda_k^h[t]\Big\}, \Big\{\lambda_{k,l}^i[t]\Big\}, \Big\{\lambda_k^V[t]\Big\}, \Big\{\lambda_l^W[t]\Big\}\Big)$$

includes the dual variables associated with constraints (16a), (16b), (15c), (21a), (21e), (21f), (24a), (24b), (24c) and two linear matrix inequalities in (15d). Let

$$\Phi(\mathbf{V}_k[t], a_i[t], b_i[t]) \coloneqq e^{a_k[t]+b_k[t]} - \mathbf{h}_k^H\mathbf{V}_k[t]\mathbf{h}_k, \tag{33a}$$

$$\Psi\big(\beta_{k,l}[t], c_{k,l}[t]\big) \coloneqq \log_2\Big(e^{c_{k,l}[t]}+1\Big) - \beta_{k,l}[t], \tag{33b}$$

$$\Theta\Big(\{\mathbf{V}_i[t]\}_{i\neq k}, \{\boldsymbol{W}_j[t]\}_{j\neq l}, d_{k,l}[t]\Big) \coloneqq e^{d_{k,l}[t]} - \sum_{i\in\mathbb{K}\setminus\{k\}} \mathbf{m}_l^H\mathbf{V}_i[t]\mathbf{m}_l - \sum_{j\in\mathbb{L}\setminus\{l\}} \boldsymbol{m}_l^H\boldsymbol{W}_j[t]\boldsymbol{m}_l - \sigma_l^2, \tag{33c}$$

that are the constraint functions associated with (21a), (21e), and (21f), respectively. Because $\{\widehat{\mathbf{u}}[t]\}$ is a KKT point of $\mathcal{P}_{1\text{-D}}$, it must satisfy the associated KKT conditions. In other words, $a_k[t]$ (see (21a) and (24a)) must satisfy

$$\frac{\partial\mathcal{L}(\{\widehat{\mathbf{u}}[t]\}, \boldsymbol{\lambda}[t])}{\partial a_k} = \lambda_k^d[t]\frac{\partial\Phi\Big(\widehat{\mathbf{V}}_k[t], \hat{a}_k[t], \hat{b}_k[t]\Big)}{\partial a_k} + \lambda_k^g[t]\frac{\partial\bar{f}_1(\alpha_k[t], a_k[t]|\hat{a}_k[t-1])}{\partial a_k} = 0 \tag{34}$$

for all $k\in\mathbb{K}$, $l\in\mathbb{L}$. Similarly, the other components of $\{\widehat{\mathbf{u}}[t]\}$ must satisfy the corresponding KKT conditions as well, in addition to that all the dual variables are either greater than or equal to zero or PSD.

Moreover, it is not hard to verify that (32a) satisfies the following properties:

$$f_1(\hat{\alpha}_k[t-1], \hat{a}_k[t-1]) = \bar{f}_1(\hat{\alpha}_k[t-1], \hat{a}_k[t-1]|\hat{a}_k[t-1]), \tag{35}$$

$$\frac{\partial f_1(\alpha_k, a_k)}{\partial\alpha_k} = \frac{\partial\bar{f}_1(\alpha_k, a_k|\hat{a}_k[t-1])}{\partial\alpha_k}, \tag{36}$$

$$\frac{\partial f_1(\alpha_k, a_k)}{\partial a_k}\bigg|_{a_k=\hat{a}_k[t-1]} = \frac{\partial\bar{f}_1(\alpha_k, a_k|\hat{a}_k[t-1])}{\partial a_k}\bigg|_{a_k=\hat{a}_k[t-1]}. \tag{37}$$

Since $\{\widehat{\mathbf{u}}[t]\}_{t=0}^{\infty}$ is bounded and $\mathcal{P}_{1\text{-D}}$ satisfies the Slater's condition, there exist a subsequence $\{t_1, \ldots, t_\rho, \ldots\} \subseteq \{1, \ldots, t, \ldots\}$ and a primal-dual limit point, denoted by $\widehat{\mathbf{u}}^\star \coloneqq (\{\widehat{\mathbf{V}}_k^\star\}, \{\widehat{\mathbf{W}}_l^\star\}, \{\hat{\alpha}_k^\star\}, \{\hat{\beta}_{k,l}^\star\}, \{\hat{a}_k^\star\}, \{\hat{b}_k^\star\}, \{\hat{c}_{k,l}^\star\}, \{\hat{d}_{k,l}^\star\})$ and $\boldsymbol{\lambda}^\star \coloneqq (\{\lambda_k^{a\star}\}, \{\lambda_l^{b\star}\}, \{\lambda^{c\star}\}, \{\lambda_k^{d\star}\}, \{\lambda_{k,l}^{e\star}\}, \{\lambda_{k,l}^{f\star}\}, \{\lambda_k^{g\star}\}, \{\lambda_k^{h\star}\}, \{\lambda_{k,l}^{i\star}\}, \{\lambda_k^{V\star}\}, \{\lambda_l^{W\star}\})$ such that

$$\lim_{\rho\to\infty}\widehat{\mathbf{u}}^\star\big[t_\rho\big] = \widehat{\mathbf{u}}^\star, \quad \lim_{\rho\to\infty}\boldsymbol{\lambda}^\star\big[t_\rho\big] = \boldsymbol{\lambda}^\star, \tag{38}$$

where $(\widehat{\mathbf{u}}^\star, \boldsymbol{\lambda}^\star)$ is primal-dual feasible to $\mathcal{P}_{1\text{-D}}$. Consider (34) for $t\in\{t_1, \ldots, t_\rho, \ldots\}$. By letting $\rho\to\infty$, and by (37) and (38), we obtain

$$\lambda_k^{d\star}\frac{\partial\Phi\Big(\widehat{\mathbf{V}}_k^\star, \hat{a}_k^\star, \hat{b}_k^\star\Big)}{\partial a_k} + \lambda_k^{g\star}\frac{\partial f_1\big(\hat{\alpha}_k^\star, \hat{a}_k^\star\big)}{\partial a_k} = 0, \tag{39}$$

which is the KKT condition associated $\mathcal{P}_{1\text{-C}}$ satisfied by $\hat{a}_k^\star$. By applying similar arguments above to all the other KKT conditions of $\mathcal{P}_{1\text{-D}}$ (that are involved with (31), (32), and (33)), we end up with the conclusion that $\widehat{\mathbf{u}}^\star$ satisfies the KKT conditions of problem $\mathcal{P}_{1\text{-C}}$. Thus, the proof is finished.

REFERENCES

[1] L. Belkhir and A. Elmeligi, "Assessing ICT global emissions footprint: Trends to 2040 & recommendations," *J. Clean. Prod.*, vol. 177, pp. 448–463, Mar. 2018.

[2] S. Buzzi, C.-L. I, T. E. Klein, H. V. Poor, C. Yang, and A. Zappone, "A survey of energy-efficient techniques for 5G networks and challenges ahead," *IEEE J. Sel. Areas Commun.*, vol. 34, no. 4, pp. 697–709, Apr. 2016.

[3] J. Ren, Y. Zhang, N. Zhang, D. Zhang, and X. Shen, "Dynamic channel access to improve energy efficiency in cognitive radio sensor networks," *IEEE Trans. Wireless Commun.*, vol. 15, no. 5, pp. 3143–3156, Jan. 2016.

[4] L. Sboui, Z. Rezki, and M. Alouini, "Energy-efficient power allocation for underlay cognitive radio systems," *IEEE Trans. Cogn. Commun. Netw.*, vol. 1, no. 3, pp. 273–283, Oct. 2015.

[5] Z. Bai, L. Ma, Y. Dong, P. Ma, and Y. Ma, "Energy-efficient resource allocation for secure cognitive radio network with delay QoS guarantee," *IEEE Syst. J.*, vol. 13, no. 3, pp. 2795–2805, Oct. 2019.

[6] *Visual Networking Index: Forecast and Trends 2017–2022*, Cisco, San Jose, CA, USA, Feb. 2019.

[7] J. Mitola and G. Q. Maguire, "Cognitive radio: Making software radios more personal," *IEEE Pers. Commun.*, vol. 6, no. 4, pp. 13–18, Aug. 1999.

[8] B. Wang and K. J. R. Liu, "Advances in cognitive radio networks: A survey," *IEEE J. Sel. Topics Signal Process.*, vol. 5, no. 1, pp. 5–23, Feb. 2011.

[9] T. Yucek and H. Arslan, "A survey of spectrum sensing algorithms for cognitive radio applications," *IEEE Commun. Surveys Tuts.*, vol. 11, no. 1, pp. 116–130, 1st Quart., 2009.

[10] Y.-C. Liang, Y. Zeng, E. C. Y. Peh, and A. T. Hoang, "Sensing-throughput tradeoff for cognitive radio networks," *IEEE Trans. Wireless Commun.*, vol. 7, no. 4, pp. 1326–1337, Apr. 2008.

[11] S. K. Sharma, T. E. Bogale, S. Chatzinotas, B. Ottersten, L. B. Le, and X. Wang, "Cognitive radio techniques under practical imperfections: A survey," *IEEE Commun. Surveys Tuts.*, vol. 17, no. 4, pp. 1858–1884, 4th Quart., 2015.

[12] D. Li, J. Cheng, and V. C. M. Leung, "Adaptive spectrum sharing for half-duplex and full-duplex cognitive radios: From the energy efficiency perspective," *IEEE Trans. Commun.*, vol. 66, no. 11, pp. 5067–5080, Nov. 2018.

[13] M. C. Filippou, D. Gesbert, and G. A. Ropokis, "A comparative performance analysis of interweave and underlay multi-antenna cognitive radio networks," *IEEE Trans. Wireless Commun.*, vol. 14, no. 5, pp. 2911–2925, Jan. 2015.

[14] J. Xiong, D. Ma, K. Wong, and J. Wei, "Robust masked beamforming for MISO cognitive radio networks with unknown eavesdroppers," *IEEE Trans. Veh. Technol.*, vol. 65, no. 2, pp. 744–755, Feb. 2016.

[15] A. G. Fragkiadakis, E. Z. Tragos, and I. G. Askoxylakis, "A survey on security threats and detection techniques in cognitive radio networks," *IEEE Commun. Surveys Tuts.*, vol. 15, no. 1, pp. 428–445, 1st Quart., 2013.
[16] T. Jiang, T. Li, and J. Ren, "Toward secure cognitive communications in wireless networks," *IEEE Wireless Commun.*, vol. 19, no. 4, pp. 82–88, Aug. 2012.
[17] Y. Zou, X. Wang, and W. Shen, "Physical-layer security with multiuser scheduling in cognitive radio networks," *IEEE Trans. Commun.*, vol. 61, no. 12, pp. 5103–5113, Dec. 2013.
[18] X. Chen, D. W. K. Ng, W. H. Gerstacker, and H. Chen, "A survey on multiple-antenna techniques for physical layer security," *IEEE Commun. Surveys Tuts.*, vol. 19, no. 2, pp. 1027–1053, 2nd Quart., 2017.
[19] H. Mu and J. K. Tugnait, "Secure degrees of freedom in MIMO cognitive radio systems," in *Proc. IEEE GLOBECOM*, 2014, pp. 1011–1016.
[20] Y. Pei, Y. Liang, L. Zhang, K. C. Teh, and K. H. Li, "Achieving cognitive and secure transmissions using multiple antennas," in *Proc. IEEE PIMRC*, 2009, pp. 1–5.
[21] Y. Pei, Y. Liang, L. Zhang, K. C. Teh, and K. H. Li, "Secure communication over MISO cognitive radio channels," *IEEE Trans. Wireless Commun.*, vol. 9, no. 4, pp. 1494–1502, Apr. 2010.
[22] Y. Pei, Y. Liang, K. C. Teh, and K. H. Li, "Secure communication in multi-antenna cognitive radio networks with imperfect channel state information," *IEEE Trans. Signal Process.*, vol. 59, no. 4, pp. 1683–1693, Feb. 2011.
[23] P. Chen, J. Ouyang, W. Zhu, and M. Lin, "Energy efficient beamforming for multi-user transmission in cognitive radio networks with secrecy constraints," *IEEE Access*, vol. 6, pp. 74485–74493, 2018.
[24] J. Ouyang, M. Lin, Y. Zou, W. Zhu, and D. Massicotte, "Secrecy energy efficiency maximization in cognitive radio networks," *IEEE Access*, vol. 5, pp. 2641–2650, 2017.
[25] J. Ouyang, M. Lin, W. Zhu, D. Massicotte, and A. L. Swindlehurst, "Energy efficient beamforming for secure communication in cognitive radio networks," in *Proc. IEEE ICASSP*, 2016, pp. 3496–3500.
[26] F. Zhou, Y. Wang, D. Qin, Y. Wang, and Y. Wu, "Secure EE maximisation in green CR: Guaranteed SC," *IET Commun.*, vol. 11, no. 16, pp. 2507–2513, 2017.
[27] Y. Jiang, Y. Zou, J. Ouyang, and J. Zhu, "Secrecy energy efficiency optimization for artificial noise aided physical-layer security in OFDM-based cognitive radio networks," *IEEE Trans. Veh. Technol.*, vol. 67, no. 12, pp. 11858–11872, Oct. 2018.
[28] L. Ni, X. Da, H. Hu, M. Zhang, and K. Cumanan, "Outage constrained robust secrecy energy efficiency maximization for EH cognitive radio networks," *IEEE Wireless Commun. Lett.*, vol. 9, no. 3, pp. 363–366, Aug. 2020.
[29] M. Gastpar, "On capacity under receive and spatial spectrum-sharing constraints," *IEEE Trans. Inf. Theory*, vol. 53, no. 2, pp. 471–487, Feb. 2007.
[30] F. Gabry, A. Zappone, R. Thobaben, E. A. Jorswieck, and M. Skoglund, "Energy efficiency analysis of cooperative jamming in cognitive radio networks with secrecy constraints," *IEEE Wireless Commun. Lett.*, vol. 4, no. 4, pp. 437–440, May 2015.
[31] W. Dinkelbach, "On nonlinear fractional programming," *Manag. Sci.*, vol. 13, pp. 492–498, Mar. 1967.
[32] B. Marks and G. P. Wright, "A general inner approximation algorithm for nonconvex mathematical programs," *Oper. Res.*, vol. 26, no. 4, pp. 681–683, 1978.
[33] C.-Y. Chi, W.-C. Li, and C.-H. Lin, *Convex Optimization for Signal Processing and Communications: From Fundamentals to Applications*. Boca Raton, FL, USA: CRC Press, 2017.
[34] H. Song, H. Wen, L. Hu, Y. Chen, and R. Liao, "Optimal power allocation for secrecy rate maximization in broadcast wiretap channels," *IEEE Wireless Commun. Lett.*, vol. 7, no. 4, pp. 514–517, Aug. 2018.
[35] D. N. Nguyen and M. Krunz, "Power minimization in MIMO cognitive networks using beamforming games," *IEEE J. Sel. Areas Commun.*, vol. 31, no. 5, pp. 916–925, May 2013.
[36] W. H. Press, S. A. Teukolsky, W. T. Vetterling, and B. Flannery, "Golden section search in one dimension," in *Numerical Recipes: The Art of Scientific Computing*, 3rd ed. New York, NY, USA: Cambridge Univ. Press, 2007, ch. 10.2.
[37] M. Zhang and Y. Liu, "Secure beamforming for untrusted MISO cognitive radio networks," *IEEE Trans. Wireless Commun.*, vol. 17, no. 7, pp. 4861–4872, Jul. 2018.
[38] Y. Lu, K. Xiong, P. Fan, Z. Ding, Z. Zhong, and K. B. Letaief, "Global energy efficiency in secure MISO SWIPT systems with non-linear power-splitting EH model," *IEEE J. Sel. Areas Commun.*, vol. 37, no. 1, pp. 216–232, Jan. 2019.
[39] Y. Wen, T. Jing, Y. Huo, Z. Li, and Q. Gao, "Secrecy energy efficiency optimization for cooperative jamming in cognitive radio networks," in *Proc. IEEE ICNC*, 2018, pp. 795–799.
[40] A. Zappone, E. Björnson, L. Sanguinetti, and E. Jorswieck, "Globally optimal energy-efficient power control and receiver design in wireless networks," *IEEE Trans. Signal Process.*, vol. 65, no. 11, pp. 2844–2859, Jun. 2017.
[41] A. Ben-Tal and A. Nemirovski, *Lectures on Modern Convex Optimization: Analysis, Algorithms, and Engineering Applications*. Philadelphia, PA, USA: SIAM, 2001.
[42] K. Wang, A. M. So, T. Chang, W. Ma, and C. Chi, "Outage constrained robust transmit optimization for multiuser MISO downlinks: Tractable approximations by conic optimization," *IEEE Trans. Signal Process.*, vol. 62, no. 21, pp. 5690–5705, Sep. 2014.
[43] M. Grant, S. Boyd, and Y. Ye. (Apr. 2011). *CVX: MATLAB Software for Disciplined Convex Programming, Version 1.21*. [Online]. Available: http://cvxr.com/cvx/.
[44] J. F. Sturm, "Using SeDuMi 1.02, a MATLAB toolbox for optimization over symmetric cones," *Optim. Method Softw.*, vols. 11–12, nos. 1–4, pp. 625–653, 1999.

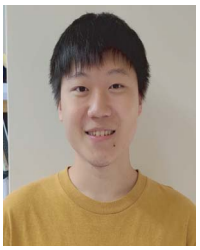

Wei-Bang Wang received the B.S. degree from the Electrical Engineering Department, National Chi Nan University, Taiwan, in 2018. He is currently pursuing the master's degree with the Institute of Communications Engineering, Department of Electrical Engineering, National Tsing Hua University, Hsinchu, Taiwan. His research interests include communication system and convex optimization.

Yang Lu (Member, IEEE) received the B.E. and Ph.D. degrees from Beijing Jiaotong University (BJTU), Beijing, China, in 2014 and 2020, respectively, where he has been a Professor in computer and information technology since 2020. From February 2016 to August 2016 and March 2018 to July 2018, he was a Visiting Scholar with National Tsing Hua University. From July 2017 to January 2018, he was a Visiting Scholar with Lancaster University. From October 2018 to October 2019, he was a Visiting Scholar with the University of Florida. His current research interests include the energy efficient communication system design and SWIPT. He serves as a Reviewer for IEEE JOURNAL ON SELECTED AREAS IN COMMUNICATIONS, IEEE TRANSACTIONS ON WIRELESS COMMUNICATIONS, IEEE TRANSACTIONS ON COMMUNICATIONS, IEEE TRANSACTIONS ON VEHICULAR TECHNOLOGY, and IEEE WIRELESS COMMUNICATIONS LETTERS.

Chong-Yung Chi (Life Fellow, IEEE) received B.S. degree in electrical engineering from the Tatung Institute of Technology, Taipei, Taiwan, in 1975, the master's degree in electrical engineering from National Taiwan University, Taipei, in 1977, and the Ph.D. degree in electrical engineering from the University of Southern California, Los Angeles, CA, USA, in 1983.

He is currently a Professor with National Tsing Hua University, Hsinchu, Taiwan. He has published more than 240 technical papers including more than 85 journal papers (mostly in IEEE TRANSACTIONS ON SIGNAL PROCESSING), more than 140 peer-reviewed conference papers, three book chapters, and two books, including a recent textbook, *Convex Optimization for Signal Processing and Communications From Fundamentals to Applications* (CRC Press, 2017), which has been popularly used in a series of invited intensive short courses at the top-ranking universities in Mainland China since 2010 before its publication. Recently, he received the 2018 IEEE Signal Processing Society Best Paper Award, entitled "Outage Constrained Robust Transmit Optimization for Multiuser MISO Downlinks: Tractable Approximations by Conic Optimization," IEEE TRANSACTIONS ON SIGNAL PROCESSING, in 2014. His current research interests include signal processing for wireless communications, convex analysis and optimization for blind source separation, biomedical and hyperspectral image analysis, and graph signal processing. He has been a Technical Program Committee member for many IEEE sponsored and co-sponsored workshops, symposiums and conferences on signal processing and wireless communications, including Co-Organizer and General Co-Chairman of 2001 IEEE Workshop on Signal Processing Advances in Wireless Communications. He was an Associate Editor for four IEEE Journals, including IEEE TRANSACTIONS ON SIGNAL PROCESSING for nine years (May 2001–April 2006, January 2012–December 2015), and he was a Member of Signal Processing Theory and Methods Technical Committee from 2005 to 2010, a Member of Signal Processing for Communications and Networking Technical Committee from 2011 to 2016, and a Member of Sensor Array and Multichannel Technical Committee from 2013 to 2018, all with the IEEE Signal Processing Society.